Copyright

by

Carlos Andres Puerta Ortega

2012

The Thesis Committee for Carlos Andres Puerta Ortega
Certifies that this is the approved version of the following thesis:

A value of information analysis of permeability data in a Carbon, Capture and Storage project

APPROVED BY
SUPERVISING COMMITTEE:

Supervisor:

J. Eric Bickel

Susan Hovorka

Varun Rai

A value of information analysis of permeability data in a Carbon, Capture and Storage project

by

Carlos Andres Puerta Ortega, B.S.

Thesis

Presented to the Faculty of the Graduate School of

The University of Texas at Austin

in Partial Fulfillment

of the Requirements

for the Degree of

Master of Arts

The University of Texas at Austin

May 2012

Dedication

To my family for their support. To God for making this possible

Acknowledgements

I would like to extend my gratitude to my advisor, Dr. J. Eric Bickel, for enlightening my path into the Decision Analysis discipline. I am equally grateful with my supervisor Dr. Susan Hovorka for her continuous support and constructive feedback throughout my graduate studies.

I would also like to thank the Gulf Coast Carbon Center (GCCC) at the Bureau of Economic Geology (BEG), University of Texas at Austin for the financial support of this research.

Abstract

A value of information analysis of permeability data in a Carbon, Capture and Storage project

Carlos Andres Puerta Ortega, M. A.

The University of Texas at Austin, 2012

Supervisor: J. Eric Bickel

Carbon dioxide capture and storage (CCS) is considered one of the key technologies for reducing atmospheric emissions of CO2 from human activities (IPCC, 2005). The scale of potential deployment of CCS is enormous spanning manufacturing, power generation and hydrocarbon extraction worldwide. Uncertainty, cost-benefit challenges, market barriers and failures, and promotion and regulation of infrastructure are the main obstacles for deploying CCS technology in a broad scale.

In a CCS project, it is the operator's responsibility to guarantee the CO2 containment while complying with environmental regulations and CO2 contractual requirements with the source emitter. Acquiring new information (e.g. seismic, logs, production data, etc.) about a particular field can reduce the uncertainty about the reservoir properties and can (but not necessarily) influence the decisions affecting the deployment of a CCS project.

The main objective of this study is to provide a decision-analysis framework to quantify the Value of Information (VOI) in a CCS project that faces uncertainties about

permeability values in the reservoir. This uncertainty translates into risks of CO2 migration out of the containment zone (or lease zone), non-compliance with contractual requirements on CO2 storage capacity, and leakage of CO2 to sources of Underground Source of Drinking Water (USDW).

The field under analysis has been idealized based on a real project located in Texas. Subsurface modeling of the upper Frio Formation (injection zone) was conducted using well logs, field-specific GIS data, and other relevant published literature. The idealized model was run for different scenarios with different permeability distributions. The VOI was quantified by defining prior scenarios based on the current knowledge of a reservoir, contractual requirements, and regulatory constraints. The project operator has the option to obtain more reliable estimates of permeability, which will help to reduce the uncertainty of the CO2 behavior and storage capacity of the formation. The accuracy of the information gathering activities is then applied to the prior probabilities (Bayesian inference) to infer the value of such data.

Table of Contents

List of Tables

List of Figures

Chapter 1. INTRODUCTION

1.1 BACKGROUND AND OBJECTIVES

Carbon dioxide capture and storage (CCS) is considered one of the key technologies for reducing atmospheric emissions of CO2 from human activities (IPCC, 2005). Of all the other greenhouse gases (GHG), CO2 is responsible for about 64% of the enhanced greenhouse effect, making it the target for mitigation of GHG (Bryant, 1997). Deep saline aquifers and existing mature oil and gas fields are attractive geological formations for the injection and long-term storage of CO2 (IPCC, 2005). While depleted oil and gas fields usually offer more data availability and expertise, their remoteness and location with respect to CO2 sources represent a disadvantage compared to unexplored saline aquifers. In contrast to depleted oil and gas reservoirs, the use of saline formations for CO2 sequestration provides the opportunity to use new formations in undeveloped regions (Keating et al., 2011). Uncertainties in reservoir properties (e.g., permeability, thickness, porosity) as well as reservoir heterogeneity will ultimately affect the injectivity, storage capacity, and costs associated with any potential sequestration reservoir.

Since the CO2 is buoyant with respect to formation fluids even at supercritical conditions, there are several trapping mechanisms that prevent migration of CO2 back to the surface; these include: (1) structural and stratigraphic trapping, (2) capillary trapping, (3) solution trapping and (4) mineral trapping (Juanes, 2010). Due to the negative consequences of an uncontrolled migration of CO2 out of the containment area (e.g. aquifers, atmosphere, producing oil and gas reservoirs), it is important to consider the risk due to CO2 leakage from the reservoir via multiple pathways (e.g. wells and faults). Monitoring is a key enabling technology that serves a number of purposes from providing

information about safety and environmental concerns, to inventory verification for national accounting of GHG emissions and carbon credit trading (Benson, 2006).

The scale of potential deployment of CCS is enormous, spanning manufacturing, power generation, and hydrocarbon extraction worldwide. However, due to the cost-benefit challenges, market barriers and failures, and promotion and regulation of infrastructure, deploying CCS technology is something that requires policy action (International Energy Agency, 2010). One of the main challenges to be addressed is providing financial instruments in order to incentivize source emitters to capture the CO2 and find partners with the experience to store it underground. Secondly, but as important, is overcoming technological and sociological barriers that work against the deployment of CCS in a broad scale. Financial incentives could be achieved through the implementation of carbon credits or tax incentives. Sociological barriers could be overcome by testing large-scale projects to prove the success of CCS in different scenarios and formations. And finally, technological barriers could be addressed by providing enough funding for research.

Once proper policies are in place, it is the CCS project operator's responsibility to guarantee the CO2 containment while complying with environmental regulations and CO2 contractual requirements with the source emitter. Acquiring new information (e.g. seismic, logs, production data, etc.) about a particular field can reduce the uncertainty about the reservoir properties and can (but not necessarily) influence the decisions affecting the deployment of a CCS project.

The main objective of this study is to provide a decision-analysis framework to quantify the Value of Information (VOI) in a CCS project that faces uncertainties about permeability values in the reservoir. This uncertainty translates into risks of CO2 migration out of the containment zone (or lease zone), non-compliance with contractual

requirements on CO2 storage capacity, and leakage of CO2 into sources of Underground Source of Drinking Water (USDW).

1.2 MOTIVATIONS FOR THE RESEARCH

VOI based on Decision Analysis theory (Bratvold et al., 2009) has applications in varied areas such as finance (Oksendal, 2005, Stibolt, 1993), supply chain (Lee et al., 2000) and bidding (Milgrom, 1982), among others. However, one of the fields where this theory has been mostly applied is in the Oil and Gas industry. Topics in this area are very diverse: dimensioning the value of the information brought by drilling an appraisal well (Demirmen, 1996 and 2001, Wills et al., 2004, Kumar and Hara, 2005) and by acquiring logging information (Aggrey et al., 2006, Branco et al., 2005, Prague et al., 2006). Seismic is one of the topics that has captured the most attention (Coopersmith et al., 2006, Ballin et al., 2004, Steagall, 2005, Wagonner, 2002, Bickel et al., 2008). Publications in the CCS field are very limited.

In one of the most recent studies on VOI in a CCS project (Sato, 2011), a deterministic scenario where a decision maker (DM) has to decide whether or not to buy certain information-gathering activity is defined. The paper depicts a logical method to obtain the VOI in a CCS monitoring setting for various levels of data-gathering accuracy. The Net Present Value (NPV) of the project is defined as an empirical dependence with the radial extent of the CO2 plume, which is assumed to be log-normally distributed. The accuracy of the information-gathering activities is assumed in order to illustrate a procedure; however, the activities lack any technical support related to the nature of the information gathering.

The main objective of this study is to perform a VOI analysis in a particular CCS project by defining some prior scenarios with different probabilities and outcomes based

on the current knowledge of a reservoir, contractual requirements, and regulatory constraints. The accuracy of the information gathering activities will be explored in detail and applied to the prior probabilities (Bayesian inference). By defining a 100% accuracy scenario, the maximum value that the operator should be willing to pay for any information gathering activity will be quantified. Finally, the construction of a model will allow the operator to decide whether to sign or refuse a contract to inject a pre-defined amount of CO2 during a fixed amount of time and if more information should be gathered before taking such a decision.

1.3 LITERATURE REVIEW AND OVERVIEW

1.3.1 VOI Definition

From an economic point of view, information is a phenomenon to reduce uncertainty. Information is needed for a variety of purposes concerning any decision making process (Repo, 1987):

- Awareness or identification of the problem
- Definition or collection of relevant information
- Development of alternative hypothesis
- Evaluation of alternatives
- Selection of optimum solution or alternative
- Implementation
- Review of the results or performance as a consequence of the implemented decision

The Value of Information (VOI) is one of the most useful applications of decision analysis theory (Bratvold et al., 2009), which considers the probabilistic and economic factors that affect decisions thus eliminating or reducing the uncertainty of such decision

(Howard, 1965). VOI analysis evaluates the benefits of collecting additional information before making a decision so that value is added by enabling the decision maker (DM) to adjust the choice to the underlying uncertainty (Bratvold et al., 2009).

A decision analysis is made up of different parts including events, probabilities, alternatives, and outcomes where the chosen alternative either maximizes satisfaction or minimizes dissatisfaction (Ang and Tang, 2007). A decision is an irrevocable choice among alternative ways to allocate resources. An outcome is a resulting state of the world (Howard, 2005). Probabilities are state of beliefs used to characterize the likelihood of an occurrence of an event relative to all other possible mutually exclusive events in the same sample space. The value of a probability is between zero and one, and the sum of probabilities for all mutually exclusive events that comprise the space is equal to one. The set of probabilities for a sample space is called a probability distribution. The distributions can also be described by either a probability mass function (PMF) or a probability density function (PDF). PMFs are applied to discrete sample spaces and PDFs are applied to continuous sample spaces (Ang and Tang, 2007).

Any attempt to collect information has value only if it meets three requirements: the information gathering exercise is relevant, material, and economic (Bratvold et al., 2009). To be relevant, the information should tell us something about what we are interested. The information should also be material, meaning it has the potential to alter our decisions. And finally, the information should be economic by creating more value than it costs.

The VOI is defined as the Certain Equivalent (CE) of a certain deal with free information less the CE without information. In other words, the VOI refers to the most a DM should pay for additional information on the distinction of interest (Bratvold et al., 2009). In the specific case of a linear utility curve (Savage, 1954), i.e. risk neutrality, the

certain equivalent is equal to the expected value (Howard, 2005) or the weighted average of a deal. The definition of risk neutrality is a robust practical assumption that is commonly used in the oil and gas industry. The VOI is then defined as the expected value with additional information minus the expected value without (Bratvold et al., 2009).

$$\text{VOI} = \begin{bmatrix} Certain\ Equivalent\ with \\ free\ information \end{bmatrix} - \begin{bmatrix} Certain\ Equivalent \\ without\ information \end{bmatrix}$$

1.3.2 Properties of VOI

Some characteristics of VOI are (Bratvold et al., 2009):

- Decision change: the test has value only if it has implications in our decisions. Therefore, simply reducing uncertainty does not create value.
- Uncertainty: increasing uncertainty in the prior distribution does not necessarily lead to larger valuations of information.
- Reliability Limits: a test that is perfectly imperfect just needs to be relabeled and could be valuable. Therefore, the lowest possible reliability for a scenario with two possible outcomes is 0.5.
- Relationship between Expected Value of Perfect Information (EVPI) and Expected Value of Imperfect Information (EVII): Sometimes the value of perfect or imperfect information is referred to as the EVPI and EVII respectively. This notation only applies to risk neutrality scenarios.
- Risk sensitivity: There is not a direct relationship between the VOI and the risk aversion.

In practice, it is very common to use the Value of Perfect Information (VOPI) or Value of Clairvoyance (VOC) to cap the economic value a DM will be willing to pay for certain information (i.e. VOI). In general, we can say that any information gathering

exercise with an economic value exceeding the VOPI does not have value to the DM as it does not meet the economic criteria. In fact, if a perfect clairvoyant appeared and offered to eliminate one or both of the uncertainties in a particular problem, he/she would be willing to receive some financial consideration (Howard, 1965). This financial consideration places an upper bound on any information gathering activity (Bratvold et al., 2009).

If a certain information-gathering activity cannot predict the state of nature with 100% confidence as a clairvoyant, then the value of this information refers to the Value of Imperfect Information (VOII), which cannot be higher than the VOPI. VOII depends on the accuracy of the information-gathering activity calculated via Bayesian inference for discrete uncertainties or a conjugate prior distribution for continuous uncertainties (e.g. porosity in an oil reservoir) (Bratvold et al., 2009).

1.3.3 Intensity of preference

The VOI in a two-act linear act (Delquié, 2008) can be evaluated in terms of the intensity of preference or the difference between the utilities of the different outcomes of a particular deal. Suppose a DM with a continuous utility function for wealth U and current wealth W faces a choice between two alternatives. By defining the VOI as the increase in expected utility from acting upon the information, the VOI will increase and reach a maximum when the best alternative is tied in preference with at least one other alternative (Delquié, 2008).

In the specific case of risk neutrality, i.e. linear utility curve (Savage, 1954), the Buying Price of a deal (BPI) - or the amount the DM would be willing to pay for the information - is equal to the Selling Price (SPI) - or the amount the DM is willing to receive for giving up access to the information - (Howard, 2005), and they are both equal

to the EVII. In the case of an exponential utility curve, which follows the delta property - the addition or subtraction of a constant will augment or reduce the CE by the same constant (Howard, 2005) - the BPI and SPI are also equal and maximal when the DM is indifferent between the two outcomes. This result is particularly important as the exponential utility function is widely used and accepted as a good approximation of risk-taking behavior in decision analysis.

Chapter 2. VOI FOR STORAGE CAPACITY IN A CCS PROJECT

2.1 PROBLEM STATEMENT

Company A, the operator of a mature and depleted oil field believed to be suitable for CO2 storage, is considering signing a contract with company B, a source of anthropogenic CO2 emissions, to inject 4 MTon of CO2 for the next 3 years. One of the main uncertainties faced by Company A is the storage capacity of the reservoir. If the targeted injection formation can store at least the contractual amount of 4 MTon of CO2, company A will receive a certain amount of money in the form of carbon credits. If the formation cannot store such quantity of CO2, company A will be obliged to pay a penalty fee due to failure to meet contractual requirements.

Company A has modeled several scenarios of CO2 migration, elevated pressure and injection volume for different estimates of permeability. Reservoir modeling suggests there it is possible that the formation will not be able to store the contractual amount of CO2 and/or that the plume will migrate outside of the lease area, in which case company A will have to pay a penalty fee and/or buy new land. The Net Present Value (NPV) of these two scenarios will be a function of the amount of CO2 injected (MTon) and the price of the carbon credit per MTon of CO2 ($/MTon) minus the respective penalty fees for failing to fulfill contractual requirements or regulatory constraints. If company A decides not to sign the contract, it is assumed that no loss or revenue will be incurred. Table 1 shows a summary of the scenarios faced by Company A.

Scenario	Definition	NPV (M$)
S1	The targeted formation can store more than the required volume of 4 MTon but the CO2 plume extends beyond the lease area	Carbon credit ($/MTon) x Contractual amount (MTon) minus cost of new land
S2	The targeted formation fails to store more than the required volume of 4 MTon while meeting regulatory constraints	Penalty Fee
S3	The targeted formation fails to store more than the required volume of 4 MTon and the CO2 plume extends beyond the lease area	Penalty Fee plus cost of new land

Table 1. Definition of possible scenarios faced by Company A

Based on reservoir modeling using log analysis regression from Spontaneous Potential (SP) and resistivity logs (Dewan, 1983) and historic data, Company A thinks that the targeted formation can store the minimal contractual amount of 4 MTon of CO2. SP regression analysis on permeability is often used in the oil industry when there is limited information about the rock characteristics other than resistivity logs. It consists of running a regression analysis on SP from resistivity logs and permeability in the wells where there is permeability data available from cores and/or logs. There is not much published documentation about this procedure because of the unclear relationship between SP and permeability from petrophysical theory.

Company A has the option to obtain more reliable estimates of permeability, which will help to reduce the uncertainty of the CO2 behavior and storage capacity of the formation. There are two possibilities being considered for such purpose:

- Mud invasion modeling using UTAPWeLS® software: UTAPWeLS® is proprietary software from the Formation Evaluation Group of the Petroleum Engineering Faculty (PGE) at UT which can be used to infer the permeability of the formations based on a modeled invasion profile (Salazar et al., 2005 and 2006). The procedure consists of adjusting the permeability of the formation in the model until the simulated resistivity curves of the model matches those from the logs. A detailed study will be developed for this purpose and presented in the body of this work.
- Acquisition of new core data: acquiring core data using this methodology has associated costs, namely the cost of getting the core while drilling or by using wireline tools (Coelho et al., 2005 and Burgess et al., 2001).

2.2 VOI ANALYSIS

2.2.1 Description and generalities of the project

The field under analysis has been idealized based on a real project located in the greater Houston area. The field is a faulted, anticlinal structure formed under the influence of a deep-seated salt dome. It is 4.3 miles long and 3.7 miles wide. Located midway between the towns of Pearland and Alvin, TX, the field is about 8 miles south of the city limits of Houston. U.S. (Figure 1). Highway 35 roughly follows the subsurface trace of the most prominent fault on this structure at the top of the Frio reservoir that bisects Hastings field into Hastings East and Hastings West fields. Several other faults

branch out from the major NW-SE-trending fault, which divides West Hastings field into 15 fault blocks.

Figure 1. Hastings field location. Source: McWilliams, 1972

The Hastings field was discovered during 1934 by Stanolind Oil Company (formerly Amoco) and the field was rapidly developed with more than 600 wells drilled within the 4,600 acre West Hastings Unit. Since many of the royalty owners owned only 10 acres each, 10-acre spacing was utilized to develop the reservoir. This has resulted in high real sweep efficiency and oil recoveries exceeding 60% OOIP. Cumulative production of 582 million barrels of oil and 2.7 billion barrels water have been produced from this high permeability (200-2000 md) Frio sandstone reservoir (Davis et al., 2011).

From wireline logs, the Frio sands of West Hastings Field are typical of most sandstone along the Texas and Louisiana Gulf Coast, where porosities are in the 28-34% range. The rock composition for this field has been extracted from the final Frio report prepared by the Bureau of Economic Geology and GCCC:

"Frio sandstone of the upper Texas Gulf Coast contains a higher percentage of quartz, less feldspar, and fewer volcanic rock fragments (quartzose feldspathic volcanic litharenite), than Frio sandstone (feldspathic litharenite) of the lower Texas Gulf Coast (Bebout and others, 1978, p. 43). The Houston delta system of East Texas underlies parts of nine counties centered on southern Harris County. The system is composed of several minor, laterally coalescent, and frequently shifting delta lobes (Galloway and others, 1982). Streams of the Chita/Corrigan fluvial system of the Catahoula Formation supplied sediment. Updip deltas exhibited wave-dominated, arcuate geometries, whereas lobate delta geometries characterized episodes of maximum progradation or an area where high subsidence rates were associated with salt-withdrawal basins (Galloway and others, 1982). As a result of switching of delta lobes, the rate of coastal progradation was slow for the Houston delta system (Galloway et al., 1982)."

The injection zone is delimited by three faults and Anahuac shale on top. Based on the hydrocarbon accumulation and the historical records of isolation between zones in both sides of the faults, it is assumed that, for pressures below the original reservoir pressure, these faults will act as a seal. Figure 2 shows a cross section of Hastings field showing the main target injection zones (Frio sands), the up-dipping nature of the reservoir, and the sealing formation Anahuac.

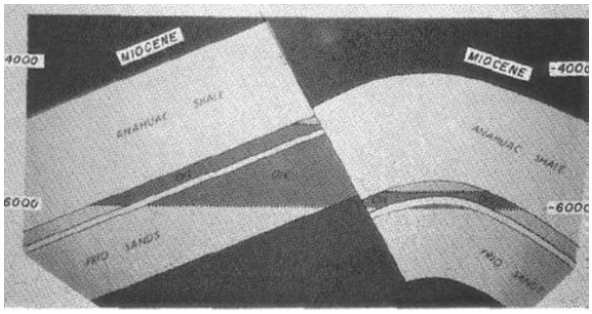

Figure 2. Cross section of Hastings Field. Source: McWilliams, 1972

The base of the Frio Formation is defined by additional shale-sandstone sequences. The Frio Formation at West Hastings field is composed of a number of sandstones separated by shales and less permeable sandstones. Multiple sandstones are productive within the field and will serve as the injection reservoir. A recent core taken across the Upper Frio Sands indicates the intervals separating the high permeability sands are actually low permeability (20-100 md), high porosity (30%) sands instead of shale, thus explaining how the high cumulative production has been obtained (Davis et al., 2011). While these tighter sands may not play a significant role during the CO2 flood, they provided additional oil that was recovered during primary conditions and have resulted in current oil saturations greater than the residual oil saturation to water in the higher permeability sands (Davis et al., 2011). The structural map at the top of the injection interval is shown in Figure 3. The square shows the idealized rectangular scenario that will be used in this analysis.

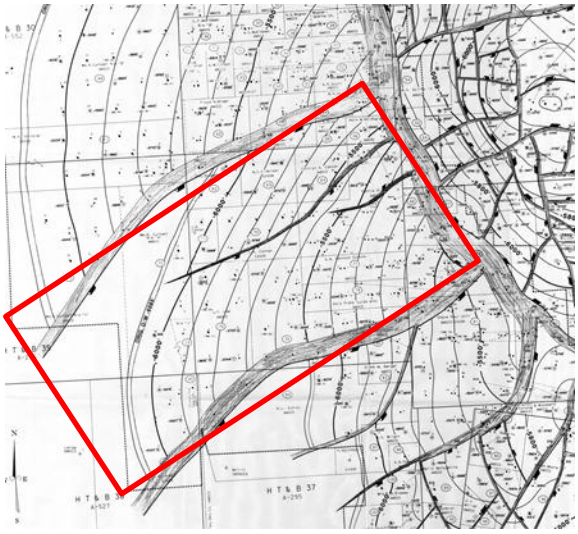

Figure 3. Structural map at top of the injection interval. Source: Texas Rail Road Commission archives

2.2.2 Geological description and initial characterization of the idealized scenario

This portion of the research was developed in conjunction with the technical team of the Gulf Coast Carbon Center (GCCC) at the Bureau of Economic Geology (BEG) (Hosseini et al., 2011).

The Frio Formation of the Gulf coastal plain is well-characterized as an injection zone, and sufficient data were publicly available to perform a basic geologic description of the Frio Formation. In addition, two sandstones of the upper Frio, in proximity to the Hastings site, were tested by the Bureau of Economic Geology (BEG) at the University of Texas at Austin during the Frio Pilot Project where 1,600 metric tons of CO2 were injected and monitored. This testing provided increased confidence during the initial characterization and modeling of the field.

Subsurface modeling of the upper Frio Formation (injection zone) was conducted using well logs from ~400 wells with ~350 digital logs (SP, RES, GR), 400 raster-image logs, field-specific GIS data, and other relevant published literature. The first step in constructing the reservoir model was to pick formation tops for the upper Frio Sand members and overlying Anahuac shale from the suite of available logs using IHS Petra® software.

To evaluate the thickness of the total sand layers in the upper Frio, net sandstone thickness was calculated by establishing a shale baseline for the given logs. Net sandstone thickness from the modeled field shows an overall shallowing and thinning trend from northwest to southeast, indicating a prograding deltaic, depositional environment. Although this process of net sand mapping is currently undergoing revision, initial interpretations show that the various upper Frio sandstones are laterally continuous, with no evidence of thinning or pinching out. Further work is needed to ensure the continuity and connectivity of these sands (Hosseini et al., 2011).

2.2.3 Dynamic modeling

A synthetic reservoir was built to simulate the process of CO2 flooding in the injection zone. The reservoir was modeled on the basis of known geology and the CO2 flood pattern design, but it was simplified to a box with a homogeneous layer. Sizing and tilting of the reservoir are listed in Table 2 (Hosseini et al., 2011).

Parameters	Value
Number of grids	25 x 50 x 17
Grid sizes (ft)	200 x 200 x 10
Dipping angles with X axis	+5
Dipping angles with Y axis	-5

Table 2. Synthetic field properties

The density of the CO2 at standard conditions 14.7 psia and 60 degF is calculated as 0.1148 lb/ft3. At a depth of 6,000 ft, the density of the CO2 at critical conditions will be approximately 700 kg/m3, assuming a typical geothermal gradient of 25 degC/km from 15 degC at the surface and hydrostatic pressure (Angus, 1973). The black-oil model CMG_IMEX® software was used to simulate the behavior of CO2 plume, the reservoir pressure, and the CO2 saturation.

Rock-fluid data (PVT table) for hydrocarbons and other properties, such as density, relative permeability curves, and compressibility come from Hastings field data. The PVTS table for CO2 comes from the template mxdrm007 in IMEX. Thirteen wells injecting at a rate of 15 MMCF/D were distributed uniformly across the area of the lease. The field is known to be producing at a residual oil saturation of about 24% (Davis et al., 2011) so the water saturation was defined as 76% above the oil-water contact. The

aquifer is assumed to be attached down dip of the oil-water contact and is treated as an infinite aquifer. The initial reservoir pressure is 2,200 psi and the model restricts the formation pressure to values not higher than 3,500 psi, at which the integrity of the seal might be compromised. Figure 4 shows the distribution of the wells in the idealized reservoir and the initial conditions for oil saturation (Hosseini et al., 2011).

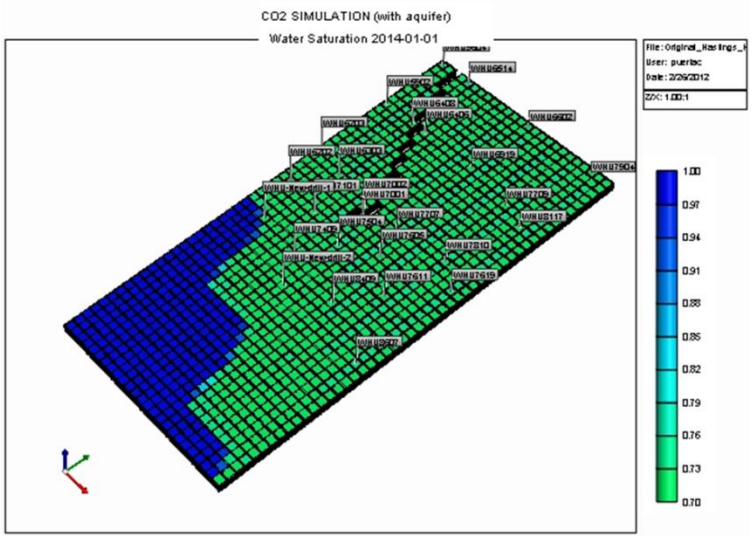

Figure 4. Idealized generic model at the beginning of the injection period (01-01-2014)

In order to quantify the VOI of permeability data, the idealized model was run for three different scenarios with different permeability distributions. For simplification purposes, these distributions were selected in a way that comprises the range of permeability values expected in the reservoir based on a nearby field.

A first idealized scenario assumes that the permeability in the X direction is equal to that in the Y direction and permeability in the Z direction is equal to that in the X direction multiplied by 0.1. It also assumes that matrix permeability varies vertically. Two permeability distributions representing highly channelized cases were created in order to account for the permeability heterogeneity in the reservoir (Hosseini et al.,

2011). Permeability values were allowed to take only three values varying from a maximum to a minimum. For example, for a particular scenario with maximum and minimum permeability values of 1000 and 100 md respectively, the model will have as input channelized compartments of 1000, 550 and 100 md (Table 3). Four additional scenarios for homogeneous permeability distributions were also simulated (10, 100, 1000 and 2000 md).

Permeability scenarios	Permeability scenario 1	Permeability scenario 2	Permeability scenario 3	Permeability scenario 4
Permeability ranges (md)	10 – 2000	10 – 100	100 – 1000	100 - 2000

Table 3. Permeability scenarios for different permeability distributions

The scenario where the permeability distribution is homogeneous in X and Z axes (Figure 5-b) is called the "best-scenario" because the created preferential flow paths lead the injected CO2 away from the aquifer. Conversely, in the "worst-case" scenario (Figure 6-b), permeability distribution favors fluid movement towards the aquifer (permeability distribution homogeneous in Y and Z axes). The results of the simulation for one of the layers in the injection zone for permeability scenario 1 and best-case and worst-case are shown in Figures 5-a and 6-a respectively. It can be observed that the distribution of the plume changes considerably with the distribution of permeability.

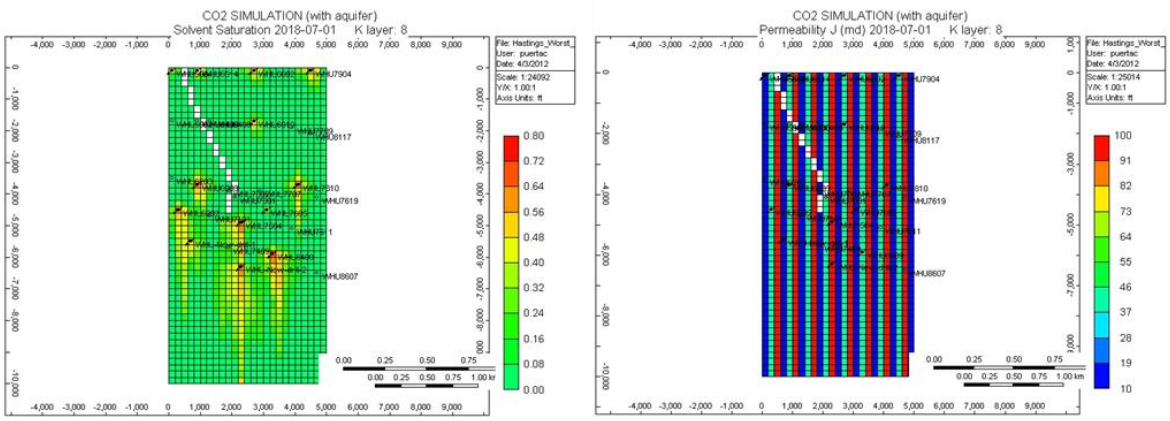

(a) (b)

Figure 5. CO2 saturation (a) and permeability (b) maps for best-case scenario

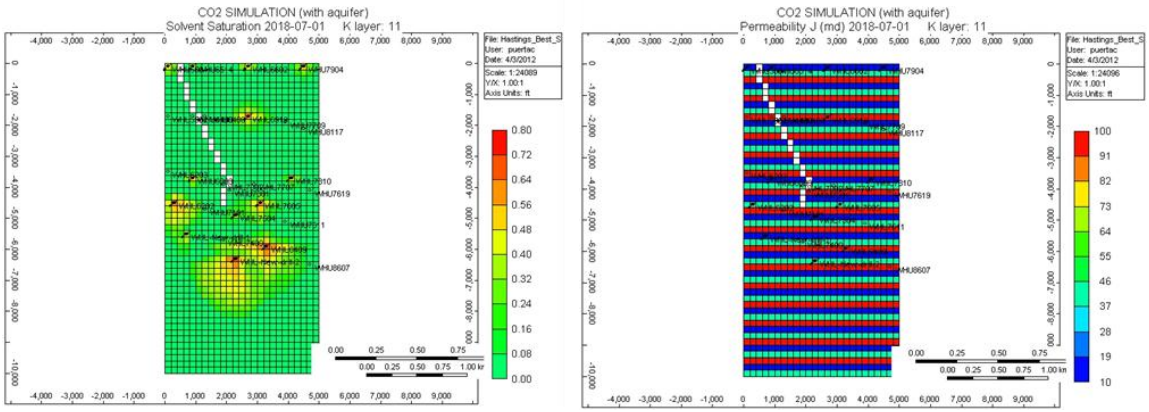

(a) (b)

Figure 6. CO2 saturation (a) and permeability (b) maps for worst-case scenario

Figure 7 shows the behavior of the Bottom Hole Pressure (BHP) and the CO2 injection rate for a particular well under the best-case permeability scenario 1. The injection rate is controlled so the BHP never exceeds a maximum limit of 3,500 psi in order to protect the integrity of the seal. The storage capacity, regardless of the permeability distribution, is significantly affected for low values of permeability as the

production rate has to be lowered in order to comply with the BHP constraint of 3,500 psi.

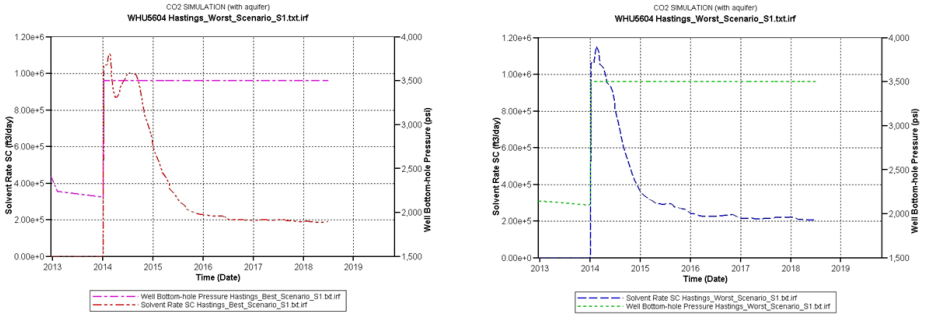

(a) (b)

Figure 7. Behavior of the Bottom Hole Pressure (BHP) and the CO2 injection rate for well 5604 under the best-case (a) and worst-case (b) permeability scenario 1

Figure 8 shows the behavior of the Bottom Hole Pressure (BHP) and the CO2 injection rate for a particular well under the best-case and worst-case permeability scenario 2. For the best-case (a) the injection rate is lowered soon after injection has started due to the poor communication of the well with the aquifer. For the worst-case (b), the injection rate can be maintained as the pressure can be more easily dissipated towards the aquifer.

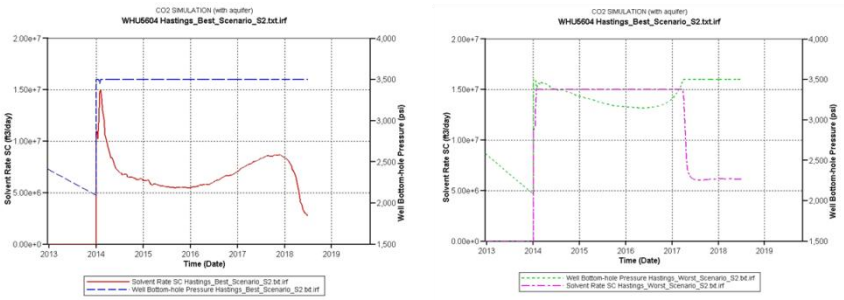

(a) (b)

Figure 8. Behavior of the Bottom Hole Pressure (BHP) and the CO2 injection rate for well 5604 under the best-case permeability scenario 1

A summary of the injection profiles for the twelve possible scenarios (four permeability scenarios for each permeability distribution) are shown in Figure 9 (a), (b) and (c). 4 MTon of CO2 with a density of 700 kg/m3 is equivalent to approximately 2.0 E+011 ft3 of CO2. Based on the graphs results, it can be inferred that up to 2017 (3 years duration of the contract), only four out of the twelve scenarios meet the storage capacity requirement of 4 MTon of CO2.

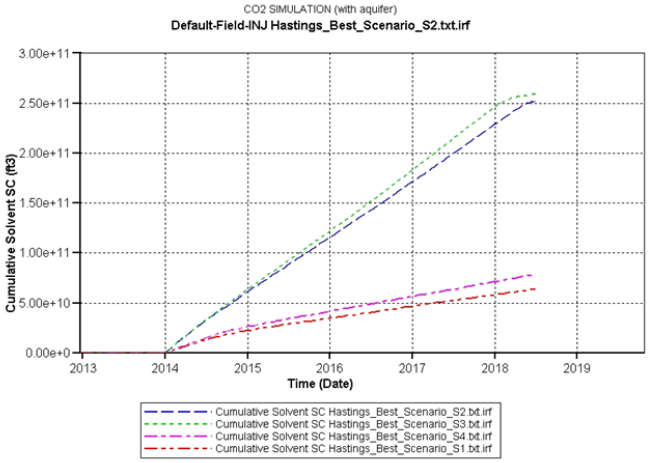

(a)

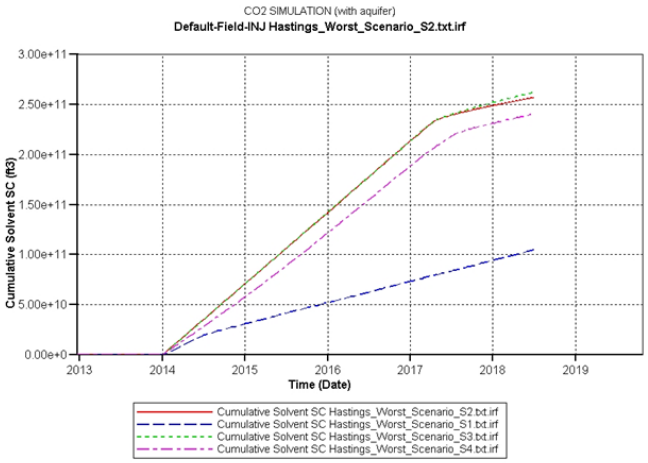

(b)

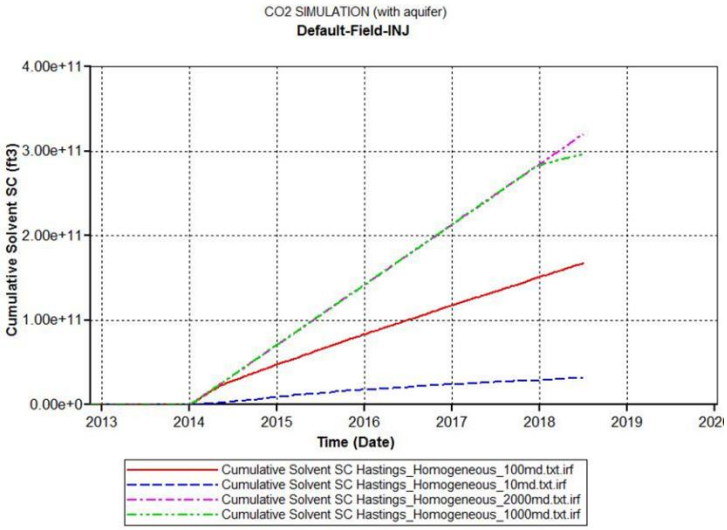

(c)

Figure 9. Injection profiles for the best-case (a), worst-case (b) and homogeneous scenarios

A summary of the results from the reservoir modeling for all the permeability scenarios is shown in Table 4. In eight out of the twelve realizations the allowable volume of CO2 injected is less than the required volume of 4 MTon, and, in two out of these eight, the CO2 plume will extend beyond the lease boundary. In the only four realizations meeting contractual storage requirements, the plume is expected to extend beyond the lease area; it is assumed that the company has the possibility to buy new land if this is the case.

No.	Permeability distribution	Values of permeability (md)	CO2 stored > 4 MTon?	CO2 plume inside lease boundary?	CO2 plume scenario	Realization No.
1	Homogeneous in X and Z directions	10 – 2000	N	Y	S2	1
		10 - 100	N	Y	S2	2
		100 - 1000	N	Y	S2	3
		100 - 2000	N	N	S3	4
2	Homogeneous in Y and Z directions	10 – 2000	N	N	S3	5
		10 - 100	N	Y	S2	6
		100 - 1000	Y	N	S1	7
		100 - 2000	Y	N	S1	8
3	Homogeneous in X, Y and Z directions	10	N	Y	S2	9
		100	N	Y	S2	10
		1000	Y	N	S1	11
		2000	Y	N	S1	12

Table 4. Summary of modeling results for different idealized scenarios and realizations

2.2.4 Set up of the decision analysis framework

2.2.4.1 Decision Trees

A decision analysis applies probabilities to various outcomes as a means to account for the uncertainty. From the assessed probabilities and associated outcomes, the

DM can evaluate whether or not implementing a certain project is preferred (Andonyadis, 2010).

A decision tree is a graphical representation of the decision making process. It lays out the events, probabilities, alternatives, and outcomes associated with the decision. In a decision tree, square nodes are decision nodes, which denote points where a decision maker makes a decision. Circular nodes are chance nodes, which represent points of uncertainty. Branches that extend from the decision nodes are alternatives and branches that extend from chance nodes are events. The expected utility for an alternative is the summation of the products of the respective probability and utility value for each event (Ang and Tang, 2007) assuming a risk neutral DM (Howard, 2005). Figure 10 demonstrates how the different components of a decision tree fit together (Namhong 2008).

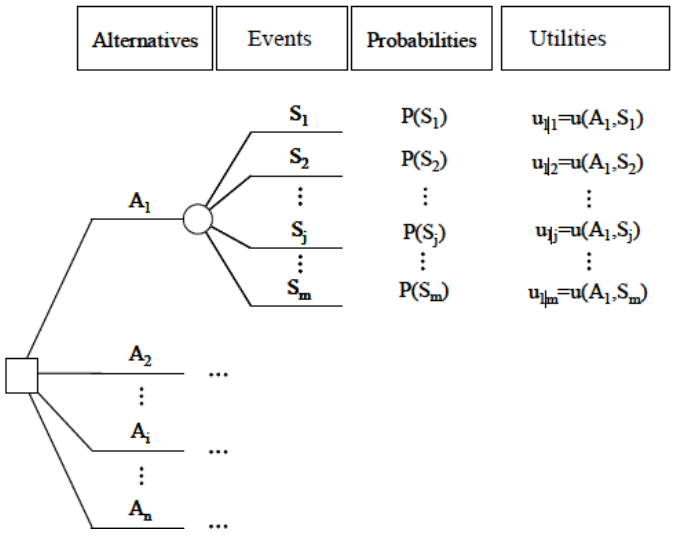

Figure 10. Basic decision tree

2.2.4.2 Relevance diagrams

One of the most useful features of decision analysis is its ability to distinguish between constructive and wasteful information gathering (Howard, 2005). A relevance

diagram (Howard and Matheson, 2005) for a typical information-gathering experimental process is shown in the upper part of Figure 5. The observed distinction is the result of the experimental process, and the value of this distinction derives from the relevance between them (Howard, 2005).

In the case of study for this report, the distinction of interest is the amount of CO2 that can be stored in the formation, and the observed distinction is the result of a permeability data study. This relevance is called the assessed form because it is the form in which probabilities representing our information are usually assessed. The conditional probability of the observed distinction given the distinction of interest is often called the likelihood. The probability distribution of the distinction of interest is usually called the prior (Howard, 2005). The reversed arrow in Figure 11 shows the inferential form of the relevance diagram and represents the probability distribution that needs to be assigned to the distinction of interest when the observed distinction is known. This is usually called a posterior distribution because it is useful after the results of the experiment are known. The probability distribution on what will be observed in the experiment is known as the preposterior (Howard, 2005).

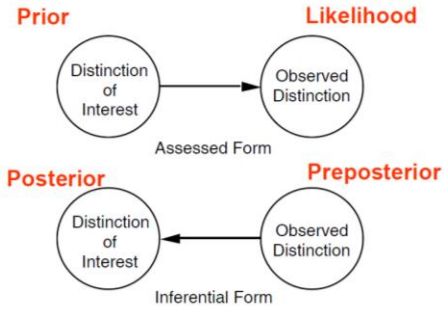

Figure 11. Relevance diagram for experimentation

2.2.4.3 Bayesian inference

The process of going from assessed to inferential form is also known as Bayesian inference. Bayes' theorem is used to relate new information to an existing probability of a sample space, to the posterior probabilities as shown in

$$p(A_i|S_j) = \frac{p(S_j|A_i)\, p(A_i)}{p(S_j)}$$

Where $p(A_i|S_j)$ is the posterior probability, $p(S_j|A_i)$ is the updated probability of event A_i given the information S_j (or likelihood), and $p(A_i)$ and $p(S_j)$ are the marginal probabilities of events A_i and S_j respectively. Based on the total probability theorem, $p(S_j)$ is defined to be

$$p(S_j) = \sum_{1}^{i} p(S_j|A_i)\, p(A_i)$$

If the likelihood distribution is uniform, then it is suggested that there is no new information that alters the original probability distribution. If the likelihood distribution applies a probability of one to a particular event but zero to all others, then it suggests perfect information, and the updated distribution only has the event occurring (Andonyadis 2010).

2.2.4.4 Influence diagrams

An influence diagram is a way of describing the dependencies among aleatory variables and decisions. An influence diagram can be used to visualize the probabilistic dependencies and to specify the states of information for which independencies can be assumed to exist (Howard and Matheson, 2005). Aleatory variables are represented by circles containing the variable name. Decisions are represented by rectangles. Results

from an information-gathering activity are represented by two concentric circles; these results are considered deterministic. An arrow pointing from an aleatory variable to a report means that the outcome of the report is influenced by the outcome of the aleatory variable. An arrow pointing from aleatory variable A to aleatory variable B means that the outcome of A can influence the probabilities associated with B. An arrow pointing to a decision from either another decision, a report, or an aleatory variable, means that the decision is made with the knowledge of the outcome of the other decision or aleatory variable. A connected set of squares and circles is called an influence diagram because it shows how aleatory variables and decisions influence each other (Howard and Matheson, 2005).

The influence diagram illustrating the decision faced by Company A is shown in Figure 12. Resistivity-SP logs and existing information about the field make the current state of the information about the field. Company A will then have the choice to acquire additional information, and if it agrees to do so, there are two sources of information available: UTAPWeLS® analysis or acquiring new core data. Once the results of the test are available, Company A will decide whether or not to sign the contract, which will ultimately influence the outcome or NPV of the decision. Note that the choice of the information gathering activity will also influence the NPV since they have different costs associated.

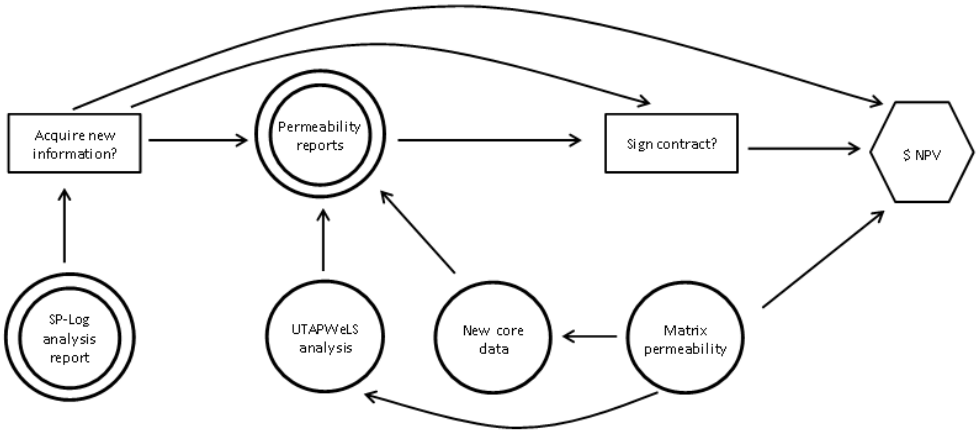

Figure 12. Decision diagram for the decision faced by Company A to sign the contract

2.2.5 Decision Analysis for the scenario with no additional information

If Company A decides not to acquire permeability tests, the decision to sign or refuse the contract must be made on prior probabilities. From the problem statement and Table 1 it is known that there are three possible scenarios S1, S2 and S3. From the results in Table 3 it can be inferred that four scenarios fall under S1, six under S2 and two under S3. As mentioned earlier, for simplification purposes, these twelve scenarios will be considered our sample space, in other words, the set of all possible outcomes of the reservoir modeling. Further, we assume that these twelve realizations are equally likely, in which case we define the probability of occurrence as (Ross, 2010):

$$p(S_i) = \frac{Number\ of\ S_i\ realizations}{12}$$

The prior probabilities for Scenarios 1, 2, and 3 (S1, S2 and S3) are then computed as p(S1) = 4/12 = 0.333, p(S2) = 6/12 = 0.500 and p(S3) = 2/12 = 0.167.

The outcome of each realization will be the NPV of the project. As defined in the problem statement, the NPV1 (NPV for scenario 1) is the Carbon credit ($/MTon) x

Contractual amount (MTon). The carbon credit received by Company A will depend on the market price of CO2 and the costs of capturing, transporting and storing technologies. Figure 13 shows suggested confidence intervals based on the Senators Lieberman and Warner's "America's Climate Security Act" (Celebi and Graves, 2003). The 90th percentile required to make CCS profitable is about \$60/tCO2. This value will be used as the market price to be received by Company B in the form of carbon credit for avoiding CO2 emissions.

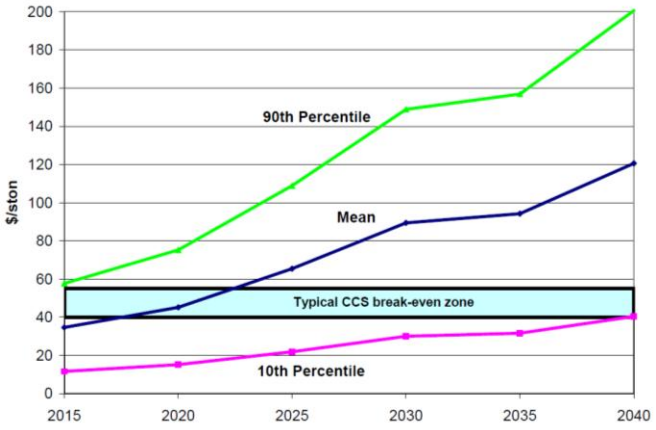

Figure 13. Confidence Interval for CO2 prices under Lieberman and Warner Act

The cost of CO2 captured is in the ranges of 11 – 32 \$/tCO2; for a pulverized coal plant this value is around \$14.55/tCO2 (Bock, 2003). The net profit for Company B will then be \$60 - \$14.55 = 45.45 \$/tCO2 captured. In order to distribute the project value and the project risk (Agarwal and Parsons, 2011), it will be assumed that 50% of the net profit of Company B (0.5 x \$45.45 \$/tCO2 = 22.73 \$/tCO2) will be allocated to Company A in order to cover the costs of transportation, underground storage, and monitoring. It is assumed that the contract has a fixed price for CO2 carbon credit. Costs for onshore CO2 transport via pipeline as function of CO2 mass flow rate are shown in Figure 14 (Bock,

2003). If the source and emitter are about 100 Km apart, the total cost of construction, operation, and maintenance will be about 3.5 $/tCO2.

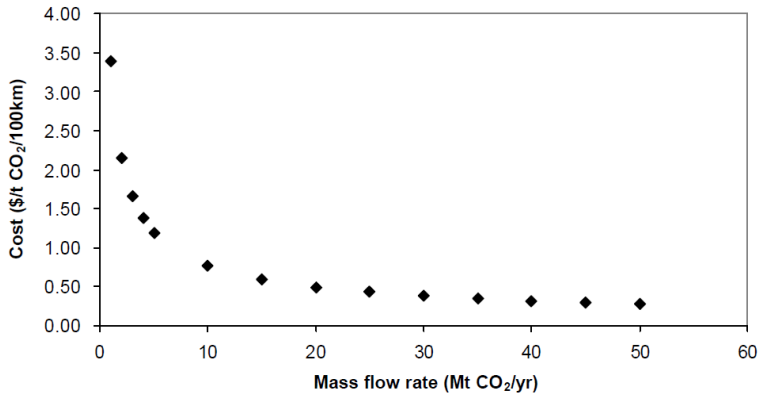

Figure 14. Total cost (construction, operation and maintenance) of onshore CO2 transport via pipeline as function of CO2 mass flow rate

A cost estimate for storage in a saline formation in USA onshore is 2.8 $/tCO2 (IPCC, 2005), and the cost of monitoring in the order of 0.2 $/tCO2. Assuming that Company A will cover the costs of transporting the CO2 from the source, the net profit for Company A will be 22.73 – 3.5 – 0.2 = 16.43 $/MtCO2. Company A has also estimated that the cost of buying new land and paying penalty fees (for the scenario where the CO2 extends beyond the lease area) is 5 M$. Consequently, and ignoring the time value of money for simplification, NPV1 = 4 MtCO2 x 16.43 $/MtCO2 – 5 M$ = 60.70 M$. The penalty fee for not meeting the contractual requirement of 4 MtCO2 has been agreed between the parties as a flat 30 M$, therefore NPV2 = -30 M$ and, NPV3 = -5 - 30 = -35 M$.

The decision tree showing the decision faced by Company A with no additional information is illustrated in Figure 15. Since the Certain Equivalent of developing the

project is negative, Company A should not sign the contract with the presently available information.

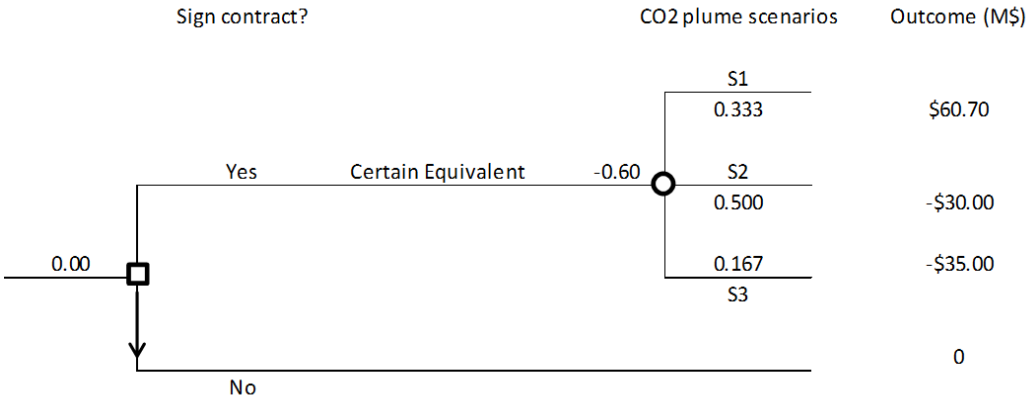

Figure 15. Decision tree showing the decision faced by Company A with current information

2.2.6 Decision analysis framework for the case with additional information

The results from an information-gathering event indicate the distribution of the properties in the reservoir but not the results of the plume scenario itself. In other words, the data report gives information about the possible realization Rj with j = 1,2,…, 12 in the reservoir but not directly about the scenario Si with i = 1,2,3 (refer to Table 3). Since the purpose of this research study is quantifying the value of permeability data, it will be assumed that the reservoir modeling in GEMS® is perfect, meaning the decisions will rely completely on the outcomes of the reservoir modeling. A schematic decision tree showing the relationship between the results of the test "Ri" with the results of the reservoir modeling "Si" is shown in Figure 16.

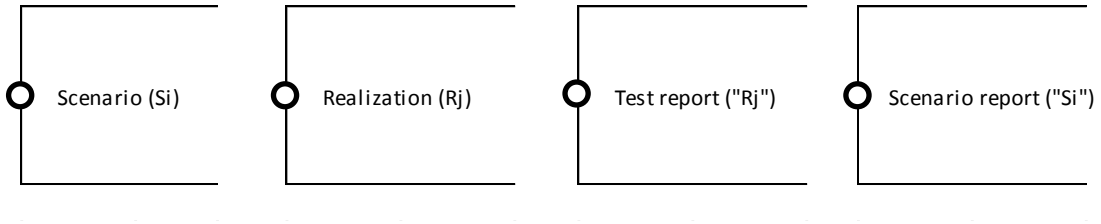

Figure 16. Schematic decision tree for Si, Rj, "Rj" and "Si"

From Table 5, scenario S1 includes realizations R7, R8, R11 and R12, scenario S2 includes realizations R1, R2, R3, R6 and R9, R10, and scenario S3 includes realizations R4 and R5 as shown in Table 4.

	R1	R2	R3	R4	R5	R6	R7	R8	R9	R10	R11	R12	Σ(Si)
S1	0	0	0	0	0	0	1	1	0	0	1	1	4
S2	1	1	1	0	0	1	0	0	1	1	0	0	6
S3	0	0	0	1	1	0	0	0	0	0	0	0	2

Table 5. Summary of realizations Rj and scenarios Si

From the table above,

$$p\left(R_j|S_i\right) = \frac{No.\,of\ realizations\ R_j}{No.\,of\ R\ realizations\ for\ scenario\ S_i}\ for\ all\ R_j \in S_i$$

$$p\left(R_j|S_i\right) = 0\ for\ all\ R_j \notin S_i$$

The test report "Rj" represents an indicator of whether the test gives a useful result or not. If the test is successful, it will predict the state of nature Rj with an accuracy

G. If the test is unsuccessful, no additional information will be obtained and the knowledge on the scenarios “Si” will be equivalent to the priors p(Si). This is:

$$p\left("R_j"\middle|R_j\right) = G$$

$$p\left("R_j"\middle|\neg R_j\right) = 1 - G$$

Based on the assumption that the reservoir modeling is 100% accurate, or p(Si) = p(“Si), the following can be said:

$$p\left("S_i"\middle|"R_j"\right) = \ 1.0 \ for \ all \ R_j \in S_i$$

$$p\left("S_i"\middle|"R_j"\right) = \ 0 \ \ for \ all \ R_j \notin S_i$$

Since the test is representative only when it reports the state of nature with G accuracy, the events "S_i" and "$\neg R_j$" are independent (Ross, 2010), therefore

$$p\left("S_i"\middle|"\neg R_j"\right) = \ p("S_i") \ = p(S_i)$$

Figure 17 illustrates the equations described above in a graphical representation in a decision tree.

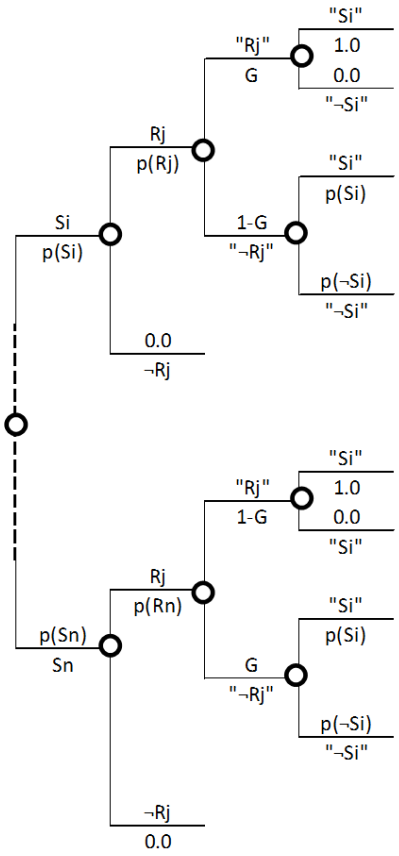

Figure 17. Decision tree showing relevance between Si, Rj, “Rj” and “Si”

By definition of conditional probability (Ross, 2010)

$$p\left("S_i"|"R_j"\right) = p\left("S_i"|"R_j"|S_i\right) p(S_i) + p\left("S_i"|"R_j"|\neg S_i\right) p(\neg S_i)$$

After performing the last computation, it is found that p(“Si”|Rj) = p(“Si”). The resulting simplified decision tree in terms of “Si” and Si is shown in Figure 18.

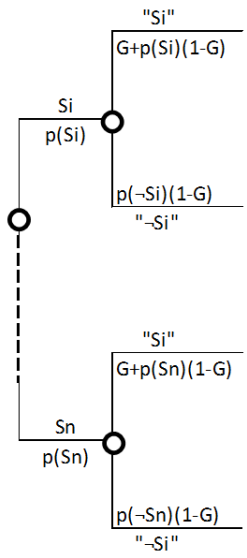

Figure 18. Simplified decision tree considering independence of events and conditional probabilities on "Rj" and Rj.

Figure 19 shows the detailed numerical exercise for S1. p(S1) represents the prior probability for S1 (4/12), since $R_7 \in S_1$, p(R7) is equal to the number of realizations of R7 over the number of realizations in scenario S1 (1/4), p("Rj") represents an assumed accuracy G=0.75 for Rj $\in$ Si and 1-G for the rest $R_j \notin S_i$. "Si" is the expected result from reservoir modeling using GEMS®.

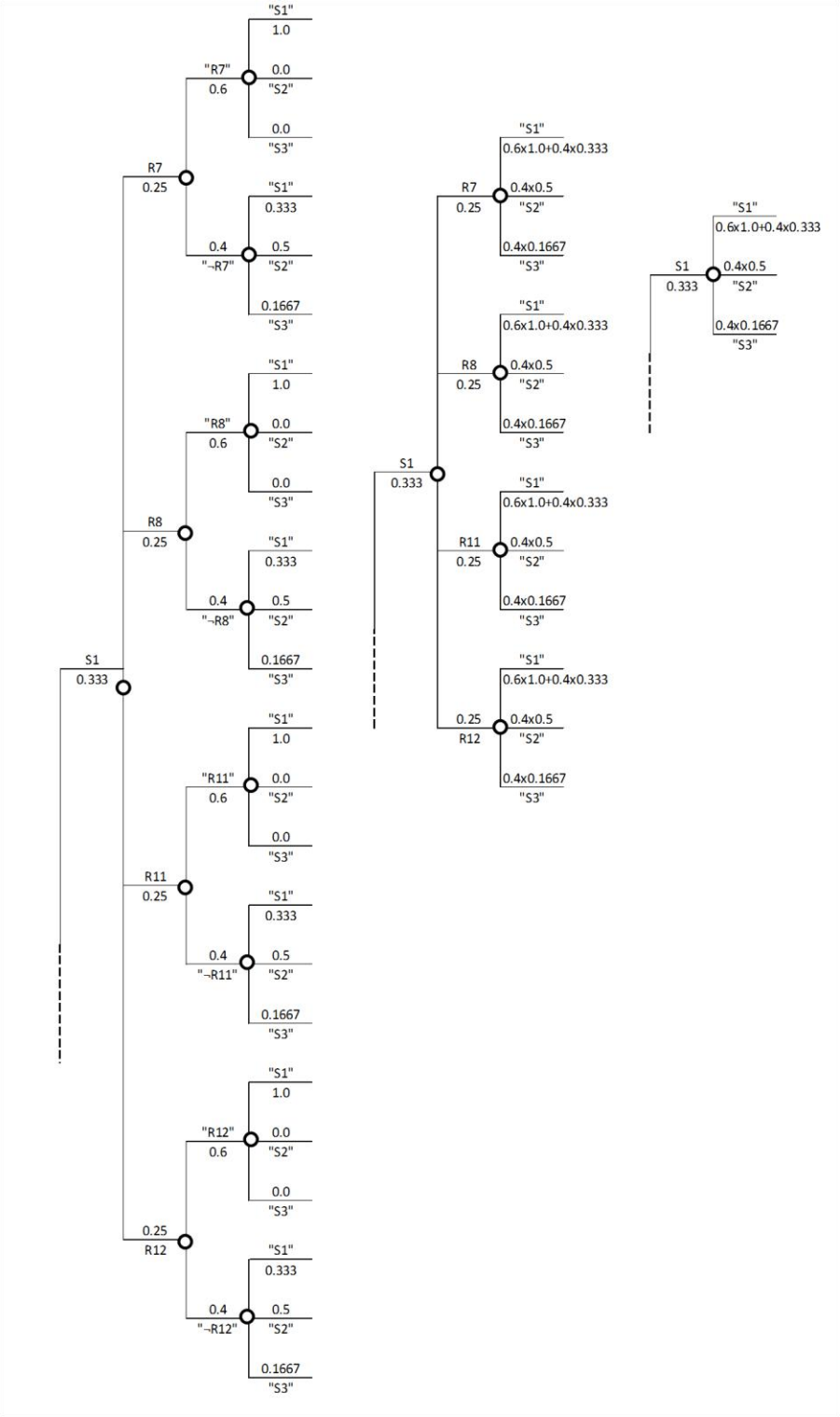

Figure 19. Numerical example of conditional probabilities for S1

2.2.7 Value of Perfect Information (VOPI)

As stated earlier, a perfect information gathering activity with G = 1.0 provides perfect knowledge of the state of the world (Bratvold et al., 2009). The VOPI places an upper limit to any information gathering activity.

As the DM will now be able to consider the decision after seeing the results of the test, the decision tree (after performing Bayesian inference) takes the form illustrated in Figure 20. If the outcome of the project is known to be S2 or S3, the DM should not sign the contract (as it is expected that the NPV realization will be negative). If the DM is certain that the S1 scenario will happen, then signing the contract will have an expected profit of 60.70 M$. However, since there is a probability of 1/3 (equivalent to the S1 prior probability) that the test reports "S1", the Certain Equivalent or Expected Value of this deal will be 20.23 M$. Since the Expected Value of the deal with no information was zero, then the VOPI is equal to 20.23 M$, and this is the maximum amount of money that company A should be willing to pay for any information gathering. If the Certain Equivalent of the deal with no information was higher than zero, then the VOPI would be the difference between 20.23 M$ and that value.

In real life, there are no such perfect tests providing perfect information. In order to account for the VOII, the accuracy of the information gathering should be quantified (Bratvold et al., 2009). As stated earlier, Company A has the option to acquire more information to improve its knowledge of the reservoir and reduce the uncertainty associated with the storage capacity and plume extent. The next chapter will explain in detail the technical details and associated accuracies of the information-gathering methodologies available.

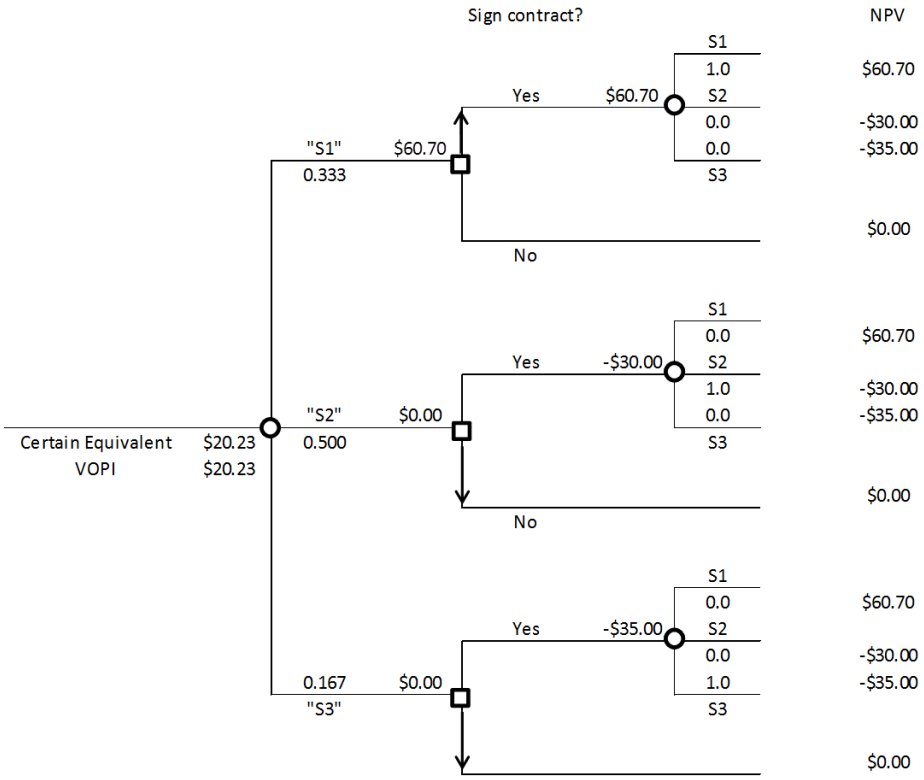

Figure 20. Decision tree to determine VOPI

2.2.8 Value of Imperfect Information (VOII)

The information-gathering activities available to Company A are punctual estimates in the area of interest or field (wells). In other words, the test reports will provide estimates of a point in the field, but an actual spatial (areal) distribution needs to be inferred from such results. If a reservoir property can be accurately mapped based on a reasonable number of collected samples, then the map can be of substantial value for site-specific management. Likewise, insufficiently intensive sampling is a waste of time and money since it does not provide the level of accuracy needed for successful site-specific management (Kravchenko, 2003).

A significant amount of research about the degree of accuracy as a function of the sampling distribution has been conducted, mainly in the agricultural and mining fields

(Kravchenko, 2003, Deutsch, 1996, Cressie and Aldworth, 1996, Humphreys, 1996, Gotway et al., 1996, Mackaness and Beard, 1988). Figure 21 (Kravchenko, 2003) shows the Goodness-of-fit of a distribution for a particular soil property in function of the number of samples and the N/S ratio (see 2.2.8.1 for definition). Figure 22 (Humphreys, 1996) illustrates the effect of the areal spacing on the variances of soil property concentrations. According to these publications, the degree of accuracy of a certain reservoir property model depends (among other factors) on the number of locations sampled. However, in these studies, the locations are usually distributed in homogeneous grids equally spaced over the area of interest, which is not always the case in an oilfield reservoir. In a particular case study presented by Deutsch, 1996, the goodness of fit (G) for a 10,000 x 10,000 ft grid was estimated as G = 0.952 for the vertically averaged porosity in a data 74 well data related to a West Texas Carbonate Reservoir. The following chapter (2.2.8.1) in this report describes the geostatistical approach for the field under analysis (Block B – 70 wells).

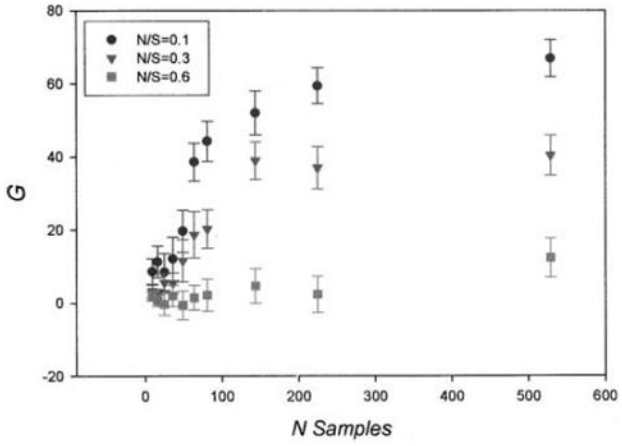

Figure 21. Average G values for different grid sizes in function of the N/S ratio.

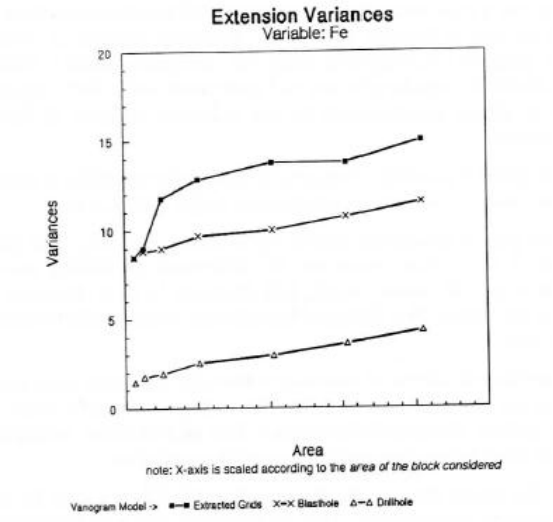

Figure 22. Variance of a soil property in function of the areal sample spacing

2.2.8.1 Geostatistical modeling of existing permeability data from cores

The permeability data available in Block B is constrained to only four wells where physical cores were taken; however, their distribution and low density make them unsuitable to perform a reliable interpolation estimate for the whole area of interest. The coordinates of the available data were transformed to a horizontal coordinate grid for simplification purposes and entered into SGeMS® software (Stanford Geostatistical Modeling Software) for further analysis (Figure 23).

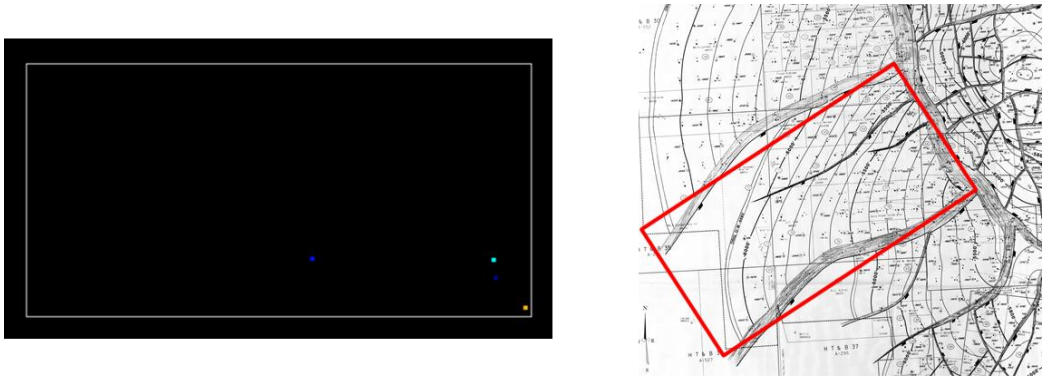

Figure 23. Block B definition in SGeMS® with available permeability values

Right next to Block B (field of interest), there is another field (Block A) with very similar reservoir characteristics and properties only separated by a structural fault. The core permeability data available from Block A will be used for the geostatistical analysis in Block B. Estimation requires a model of how a phenomenon behaves at locations that have not been previously sampled (Isaaks and Srivastava, 1989). Spatial structure in data distribution is described using a geostatistical characteristic called a variogram (Kravchenko, 2003), which is a measure of the "geological variability" vs. distance, or the expected squared difference between two data values separated by a distance vector h (Gringarten and Deutsch, 2000). The model to be used in this report will be the 2D variogram.

The locations where there is permeability data available in block A is shown in Figure 24. The values of permeability across formations in the vertical axis (depth) were averaged, and this average was used as the estimate of permeability for the entire well. The histogram and cumulative distribution functions for permeability values in Block A are shown in Figure 25.

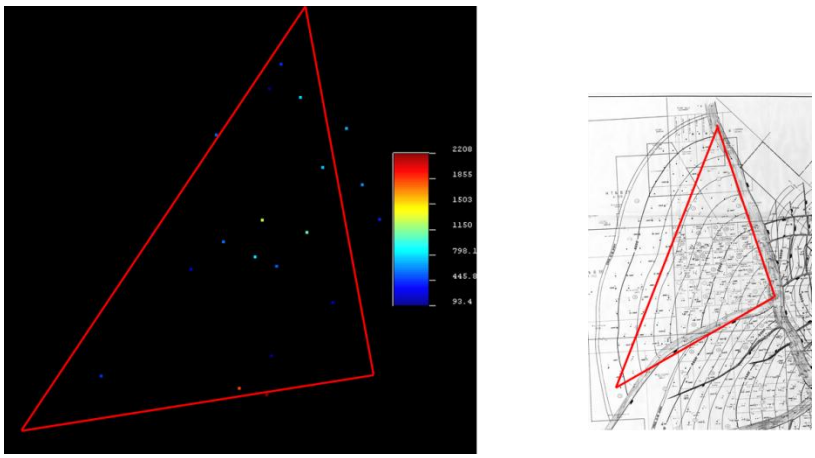

Figure 24. Block A definition in SGeMS® with available permeability values

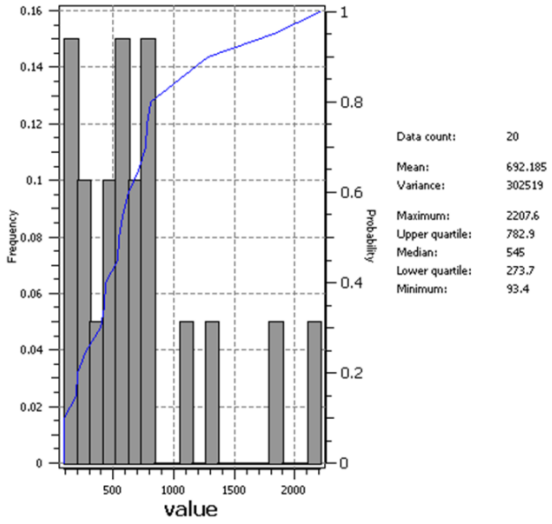

Figure 25. Histogram and cumulative distribution functions for permeability values in Block A

The variogram calculation from core data in Block A was completed by adhering to the following steps (Isaaks and Srivastava, 1989):

- Choosing the distance parameters lag spacing and tolerance: trial and error approach until an acceptable pattern is obtained.
- Finding the anisotropy axes: first an omnidirectional variogram was created and from there, a maximum trend of continuity was found at 135° Azimuth.
- Choosing the directional tolerance as 45°.

The resulting variogram is shown in Fig 26. The variogram was fit to a spherical model, which describes a random function (permeability) that is quite erratic over short distances (Isaaks and Srivastava, 1989). The Nugget (N) to Sill (S) ratio is an indicator of short-range variability that cannot be described by a geostatistical model, and the spatial correlation range defines the distance over which reservoir properties are correlated with each other (Kravchenko, 2003). The results from block A (N/S ratio 0.1/0.9 ≅ 0.11 and

range 3800 ft) suggest that higher accuracy can be achieved in mapping the variable of interest (permeability) over the extent of the reservoir (5000 ft x 10000 ft).

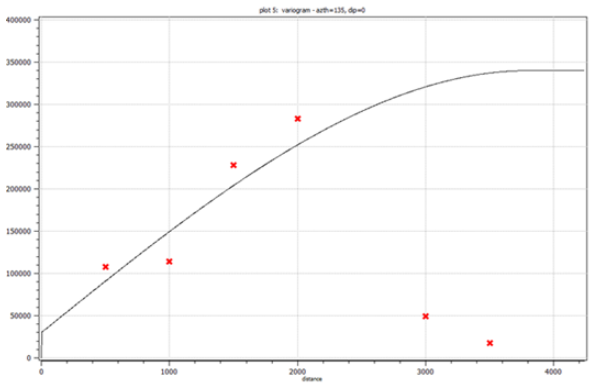

Figure 26. Variogram for available permeability data in Block A

2.2.8.2 Estimation of global permeability distribution using an indicator

Using the previous results, the following procedure was performed iteratively:

1. Generate 50 Gaussian realizations in a 10,000 pixels grid using the permeability histogram and variogram from Block A and assigning hard data from 4 cored wells in Block B (field under study).

2. Find the average value of permeability for each point in the grid across the 50 realizations.

3. For each point in the grid find the number of realizations (out of the 50) that have an average of permeability higher than a cut-off value or indicator (Isaaks and Srivastava, 1989) defined as the 90% percentile of the histogram of the hard data in Block B (900 md).

4. Take note of the sum of points across all realizations from point 3.

5. Select a point in the grid (different or not close to existing hard data points from previous realizations) whose 90% percentile of the histogram for individual data points in Block A (1500 md) across all realizations is maximum or high.

6. Use the average permeability in the location selected in step 4 as a new restriction (hard data for Block B) for the next iteration.

7. Repeat steps 1 to 6 for 70 points in the grid (or new wells).

Some of the Gaussian realizations obtained in each of the 70 iterations are shown in Figure 27.

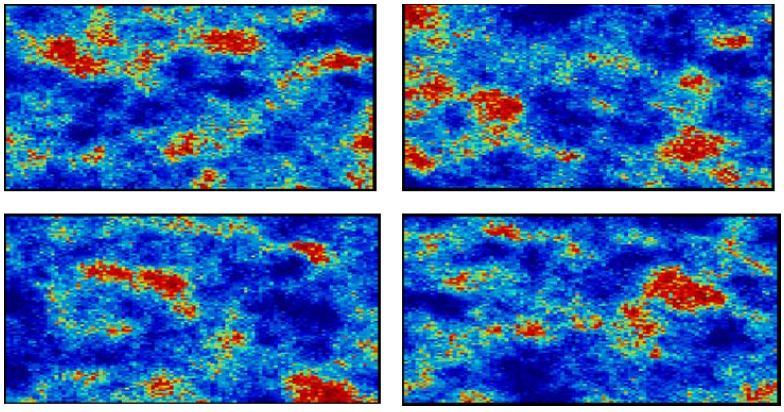

Figure 27. Gaussian realizations using the permeability histogram and variogram from Block A and assigning hard data from 4 cored wells in Block B

2.2.8.3 Data sufficiency estimation

The values obtained in step 4 were fitted to a Gaussian-type curve (Figure 28) that can be expressed as,

$$G = 1{,}400 - (1{,}400 - 46)e^{\frac{-0.8\,n^2}{39^2}} \qquad (1)$$

where n = number of wells logged/cored

It can be observed that after drilling about 80 wells, the number of values above the indicator start to converge to a value (asymptote), meaning that drilling more wells

does not significantly change the estimates of the permeability distribution in the reservoir. This result is encouraging given that there are about 70 existing wells in the field of interest that could be potentially logged or cored using wireline tools (Burgess et al., 2001) or by the execution of mini-DST tests (Coelho et al., 2005). However, this result rules out the option of drilling to acquire new core data given the high amount of wells and therefore high costs (assuming a cost of about $1 million/well) that would be incurred before a minimal degree of accuracy (i.e. accuracy values for which VOI > 0) is achieved.

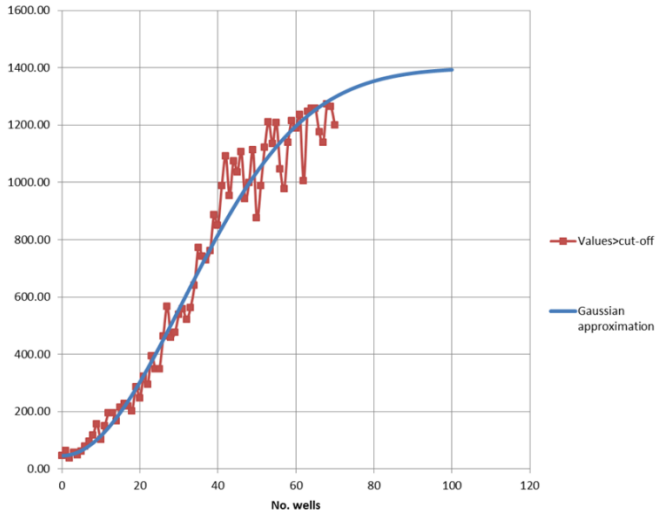

Figure 28. Gaussian type approximation for a permeability indicator of 90% percentile over the average of 50 realizations (900 md)

The accuracy of the permeability estimates was evaluated in terms of the Goodness of fit (Deutsch, 1996) of the permeability distributions for the number of wells under analysis (70 wells). Reliable probabilistic models must be both accurate and precise. A probability distribution is said to be accurate if the 10% symmetric probability interval (PI) contains the value 10% (or more) of the time, the 20% PI contains the true value 20% (or more) of the time, and so on for increasingly wide probability intervals.

Precision is a measure of the narrowness of the distribution. Precision is only defined for accurate probability distributions. A probability distribution where the 90% PI contains the true value exactly 90% of the time is said to have optimal precision (Deutsch, 1996).

A graphical way to check the assessment of accuracy is to cross plot a PI indicator function (Deutsch, 1996) versus different PI's to identify points falling above or on the 45° line. Assuming that the permeability values in Block A are the true values for permeability distribution, an accuracy plot was created for the permeability distribution for 70 (Figure 29). The Goodness of fit for this permeability distribution was calculated as G = 0.834.

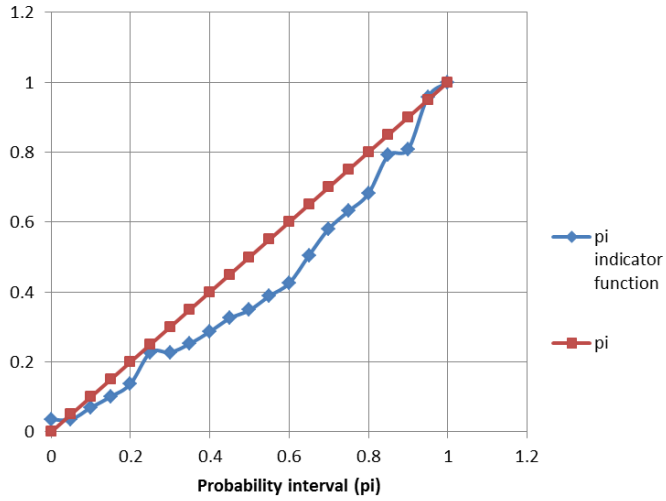

Figure 29. Accuracy plot for the permeability distribution for 70 wells

The Goodness of fit as a function of the number of wells sampled is dependent on the location or distribution of those wells spatially. In this report, such criterion relied on the locations where high permeability was expected based on 50 Gaussian simulations. Another approach based on the locations with minimum entropy (Ang and Tang, 2007) could have been used.

The optimization of the wells' location in order to characterize the reservoir is outside of the scope of this report. It is assumed that the shape of the curve Goodness of fit vs. number of wells follows the trend of the Gaussian approximation (equation 1) normalized (between 0 and 1) with G = 0.834 for 70 wells (Figure 30). As stated earlier, G = 0 (no wells logged/cored) means a state of information equivalent to the prior probabilities. The graph of G can be expressed in terms of the equation,

$$G = 1 - e^{\frac{-0.557\, n^2}{39^2}}$$

where n = number of wells logged/cored

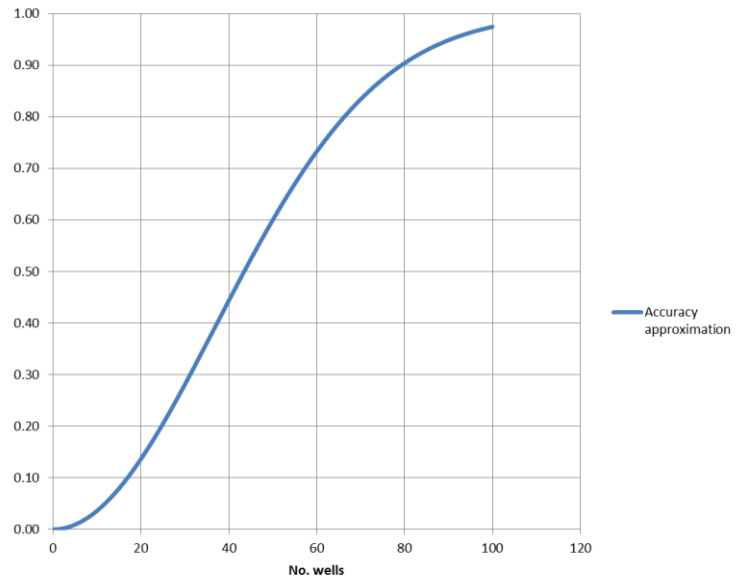

Figure 30. Accuracy as a function of number of wells from Gaussian approximation

With an estimate of the accuracy of a permeability model as a function of the number of wells available, the next step is quantifying the VOII of the two information-gathering activities accessible to Company A (UTAPWeLS® and logging/coring) in the context of the individual accuracies for each methodology and the associated costs.

2.2.9 Permeability estimation from mud invasion modeling using UTAPWeLS® and Interactive Petrophysics® software

Sufficient permeability information for reservoir characterization and monitoring is not readily available in the injection zone due to the unavailability of core and logging data (other than basic Resistivity-SP log). For this reason, an analysis of the mud invasion was performed in order to obtain permeability estimates. The methodology can be summarized as follows (Salazar et al. 2005 and 2006):

1. Perform a petrophysical characterization of the wells with a basic suit of density-porosity-resistivity-GR logs (key wells) from a nearby field.

2. Invasion modeling and inversion for the key wells in UTAPWeLS® in order to infer absolute permeability. These wells will then be used to calibrate the invasion profile in other wells with minimal SP-Resistivity data in the injection zone.

3. Run the invasion modeling and invasion in UTAPWeLS® for the wells with SP-Resistivity data in the injection zone by assuming the porosity, capillary pressure, and relative permeability curves remain the same in the production sands.

2.2.9.1 Petrophysical characterization of the key wells using Interactive Petrophysics® (IP) software

Neutron porosity: the neutron porosity data was used only to calibrate the percentage of shale (Vsh) along with the density. The neutron porosity data itself was not used as input for the water saturation (Sw) analysis, and the density data was used instead.

GR-SP: GR and SP data are coherent with the lithology and density-porosity data in all the wells except when the hole conditions were not optimal (e.g. washouts, caves). Vsh was computed using GR, SP, and Neutron-Density separately, and Vsh from GR (VshGR) was used as input for the Sw analysis. In cases when the GR was missing some

clear sands, the Vsh Average (from SP, GR and Neutron-Density) was used instead. After several trials/errors and correlation between different wells, the values to compute Vsh from Neutron-Density were: Neutron Clay = 0.43 porosity units (pu) and Density clay = 2.26 g/cc.

Water salinity: The water salinity was computed from the apparent water resistivity and borehole temperature (assumed to be equal to formation temperature) in a clear sand (i.e. 100% sandstone and 100% water-filled) using Gen-9 chart from the Schlumberger Log Interpretation charts. The inputs to calculate the water resistivity are total porosity (ϕ_t), formation resistivity (Rt), cementation factor (m), saturation exponent (n), and tortuosity factor (a), where porosity and resistivity are inputs from electrical logs. The values for these constants were estimated as m = 1.8, n = 1.7 and a = 1.

The results of the dual water analysis for several wells are coherent with minimal differences mainly due to the value of Rt, which varies due to different depths of investigation among difference resistivity tools (from different logging companies). Since Rt was not provided as part of the digital logging data, the deepest depth of investigation was used as an approximation. The water salinity values used for the water saturation analysis were:

- Free water resistivity: 0.03 ohm-m @175 degF (equivalent to a salinity of approx. 110,000 ppm in the reservoir according to the Schlumberger Log Interpertration charts, Chart Gen-9)
- Bond water resistivity (shales): 0.07 ohm-m @ 150 degF

Water saturation analysis: The Dual Water methodology (Ellis and Singer, 2008) takes the resistivity of free water in the reservoir and bond water in shale as input to compute the water saturation. The formation resistivity Rt was approximated to the deepest resistivity curve from logs. The temperature gradient was computed from the

Borehole Temperature (from logs also) assuming it changes linearly to surface temperature. This analysis did not show the presence of free gas in the sands under analysis.

Core data: a key well core porosity data was plotted against the total porosity from the Dual Water analysis; there is a good match between these two values (Figure 31). The core permeability ranges from 100 to 2500 md approximately in the target sands.

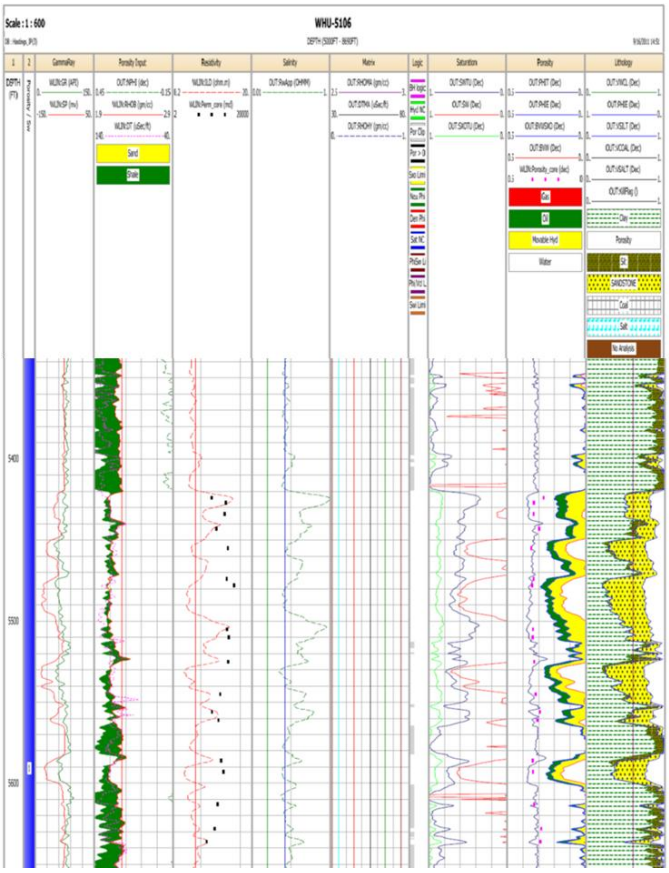

Figure 31. Petrophysical interpretation for a key well in a nearby field

2.2.9.2 Invasion modeling for key wells in UTAPWeLS® software

The values of Shale content (Csh), Water Saturation (Sw), and porosity (ϕ) obtained in the previous petrophysical analysis were used as input for the invasion

modeling. The generalized Timur-Tixier equation was used in order to infer an initial guess of the value of the permeability (k). This equation defines the relationship between k (md), Csh (fraction), Sw (fraction), and ϕ (fraction) by

$$k = A\,\frac{\phi^{B}}{S_{wirr}^{C}} \qquad (1)$$

The irreducible water saturation S_{wirr}^{C} was computed from (Dewan, 1983)

$$S_{wirr} = C_{sh□}\,\frac{\phi_{ts□}}{\phi_t}$$

where ϕ_t is total porosity and $\phi_{ts□}$ is total shale porosity. ϕ_t and $C_{sh□}$ are an output available from the petrophysical characterization performed earlier as well as the constant $\phi_{ts□}$ = 0.26.

The core data and petrophysical interpretation from the key well was used to infer the initial value of the permeability (Table 6). At each core depth, S_{wirr} was computed using equation (1). The Timur-Tixier formula obtained by a multilinear regression analysis is given by

$$k = 5.81E09\,\frac{\phi^{14.23}}{S_{wirr}^{0.215}}$$

Permeability (md)	Total porosity (%)
185	26.9
950	33.1
850	33.4
320	29.6
1200	34.8
1050	33.4
2500	34.1
1100	33.6
1350	33.8
1250	32.9
490	31.9
190	29.3
400	30.9
560	33.7
710	33.6

Table 6. Core and porosity data for key well

Radial grid and vertical flow units: Simulation of mud-filtrate invasion is performed assuming cylindrical flow and radial rock properties isotropy. The vertical grid consists of thin numerical layers to ensure high accuracy in the estimation of the flow rate of mud-filtrate invading the formation. A modified Lorenz plot (Gunter, 1997) was used to identify individual flow units in the formations under analysis. Figure 32 shows one such plot, describing the relationship between cumulative porosity and cumulative permeability as a function of reservoir thickness.

The injection zones can be identified as those with the highest slopes (better capacity of flow). The storage capacity curve does not exhibit significant changes; this is expected as the range of porosities in the interval under analysis is only about 0.28 to 0.36 (and only 0.34-0.36 in the production sands). The flow capacity curve for permeability displays changes thorough the interval, but these correspond mainly to

changes in the lithology between the production zones. In the sands the curve has a constant and steep slope, which implies that there is good capacity for flow and no significant sub-flow units within the same production interval.

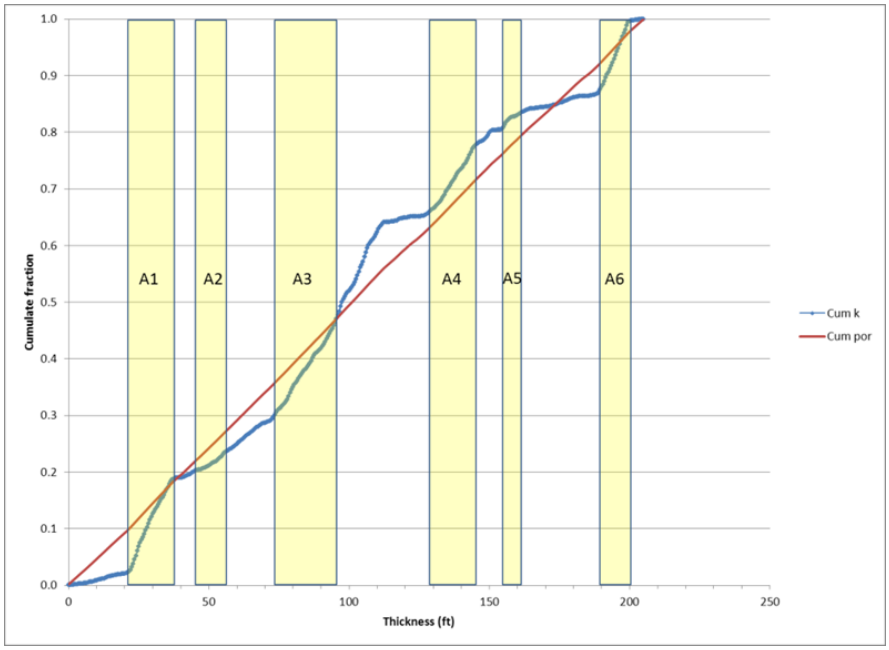

Figure 32. Modified Lorentz plot used to identify individual flow subunits. In the sands (yellow zones) the storage capacity curves cumulative (ϕ) and cumulative (k) do not exhibit significant changes within the same production interval.

Capillary pressure and relative permeability: Brooks-Corey two phase equations (Corey, 1994) were used to assign water-oil capillary pressure curves to each petrophysical layer. The equation for the capillary pressure curve is given by

$$P_c = P_c^o \sqrt{\frac{\phi}{k}} \, (1 - S_N)^{e_p}$$

where P_c is capillary pressure, P_c^o is the coefficient for capillary pressure, e_p is the pore-size distribution exponent, and S_N is the normalized wetting phase saturation given by

$$S_N = \frac{S_w - S_{wr}}{1 - S_{wr} - S_{nwr}}$$

where S_{wr} and S_{nwr} are the residual wetting (water) and non-wetting (oil) phase saturations, respectively. Capillary data from Holtz et al. was used to infer the empirical coefficients P_c^o and e_p. The results obtained for P_c^o = 8225 psi and e_p = 50.4 are shown in Figure 33.

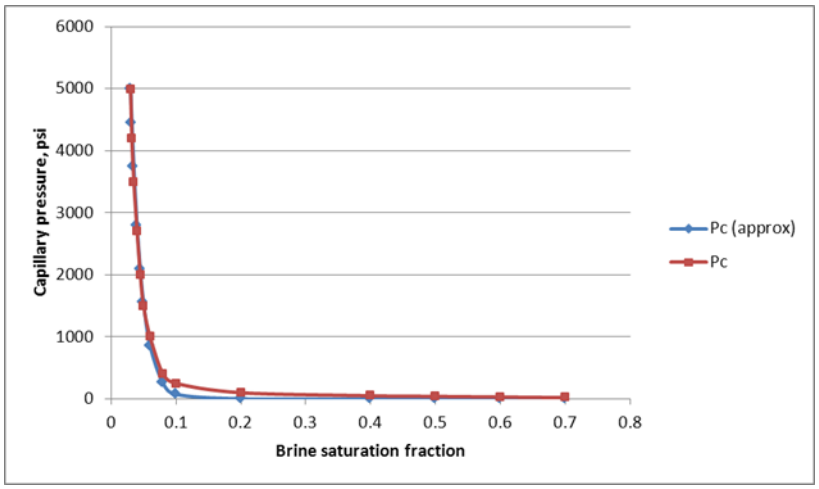

Figure 33. Graphical description of the Brooks-Corey water-oil relative permeability curves used to perform the simulation of mud filtrate invasion

Estimated relative permeability curves are shown in Table 7. The data corresponds to the results of 10 bottom hole fluid analyses from unspecified wells. Water-oil relative permeability curves in the saturated zones are also estimated via Brooks-Corey's equations given by

$$k_{rw} = k_{rw}^o S_N^{e_w}$$

and

$$k_{rnw} = k^o_{rnw}(1 - S_N)^{e_{nw}}$$

Where k_{rw} and k_{rnw} are wetting and non-wetting relative permeabilities, k^o_{rw} and k^o_{rnw} are relative permeability end points, and e_w and e_{nw} are empirical exponents for each fluid phase. The results obtained for k^o_{rw} = 0.193, k^o_{rnw} = 0.840, e_w = 4.0 and e_{nw} = 2.98 are shown in Figure 34.

Water saturation	Water relative permeability	Oil relative permeability
0.220	0.00013	1.00000
0.250	0.00062	0.84000
0.320	0.00328	0.68400
0.400	0.00908	0.42000
0.500	0.02565	0.23900
0.600	0.06375	0.10950
0.660	0.10650	0.02820
0.710	0.15950	0.00772
0.740	0.19250	0.00020

Table 7. Relative permeability data for key well

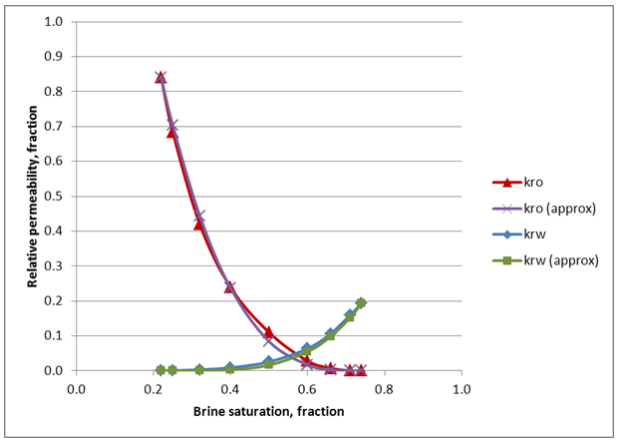

Figure 34. Graphical description of the Brooks-Corey water-oil relative capillary pressure curves used to perform the simulation of mud filtrate invasion

Static invasion model: The static model assumes two radial zones: the mud filled borehole, and the formation which is assumed to have a homogeneous invasion profile. The target zones are divided into several petrophysical layers based on the lithology and changes in resistivity. Table 8 is a summary of the average petrophysical properties calculated for the interval under study.

		Formation					
Variable	Units	1	2	3	4	5	6
Thickness	ft	20	15	25	15	15	20
Total porosity	fraction	0.36	0.34	0.35	0.34	0.36	0.36
Water saturation	fraction	0.7	0.74	0.73	0.74	0.69	0.75
Shale concentration	fraction	0.12	0.16	0.05	0.05	0.13	0.05

Table 8. Average petrophysical properties for the interest zones in key well

For each layer, an Earth Model was reproduced taking as input the $C_{s\square}$, ϕ_t and S_w values from the previous petrophysical characterization. The values of the formation resistivity from the Earth Model agree with the deep resistivity curve ILD from the logs (Figure 35). The right three tracks display the $C_{s\square}$, ϕ_t and S_w from the petrophysical characterization using IP®. The second track from the left shows the resistivity logging ILD overlapping with the formation resistivity curve from the Earth Model. The first track to the left shows the GR, SP, and CALI data from wireline logs.

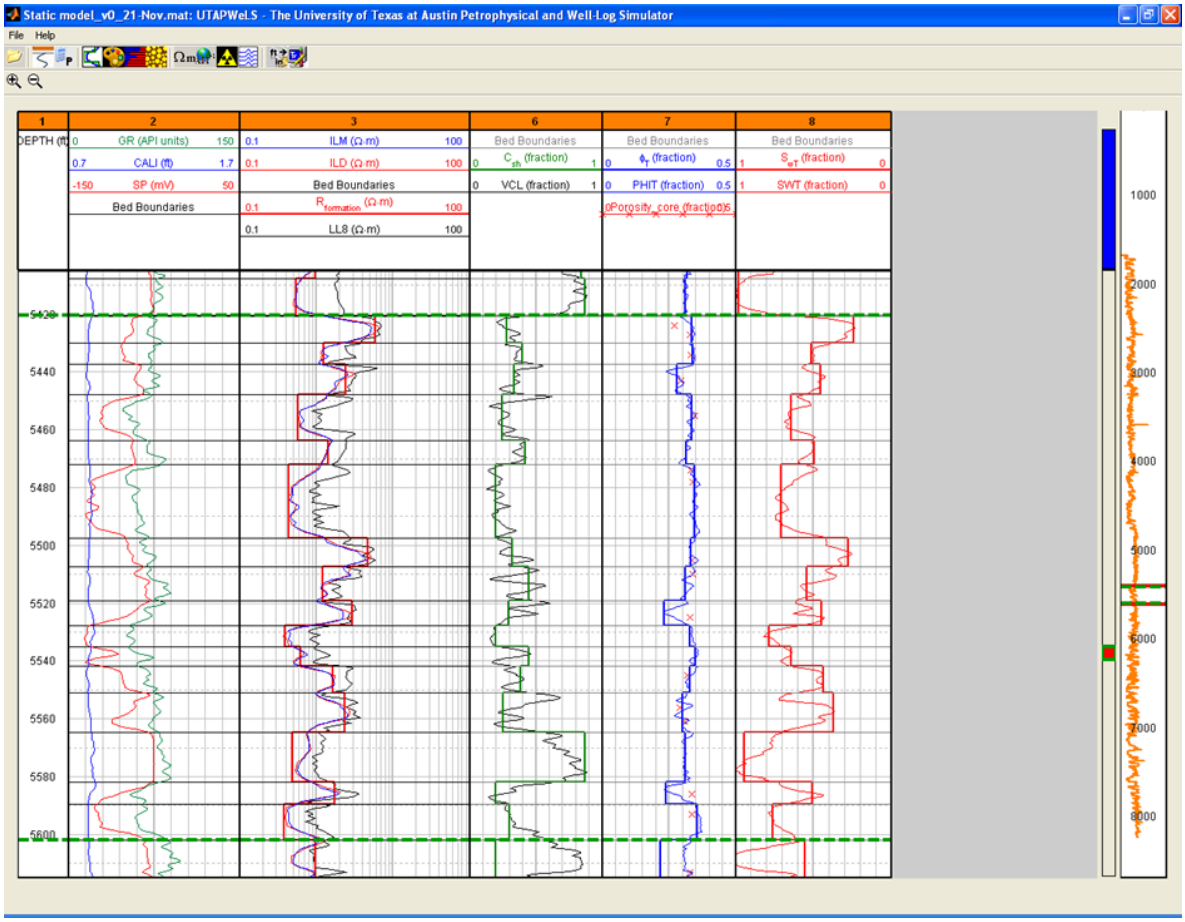

Figure 35. Result of the static model simulation in UTAPWeLS® for the formation resistivity curve

A simulated log was created for a DIT (mark of Schlumberger) resistivity tool (Figure 36). The second track from the left shows the resistivity from log data (ILD and ILM) overlapping with the results of simulated data based on the Earth Model for an DIT* tool using UTAPWeLS® (20 khz ILD and 20 khz ILM). The simulated 20 khz ILD (60 in depth of investigation) and 20 khz ILM (40 in depth of investigation) curves corrected by bed-boundary effects resemble the readings from wireline logs in all the petrophysical layers. The static model assumes that the invasion profile does not change radially and sets the initial conditions for the next step The dynamic simulation analysis

that takes into account the behavior of the mud filtrate and the amount and rate of mud cake being created which will ultimately control the invasion profile.

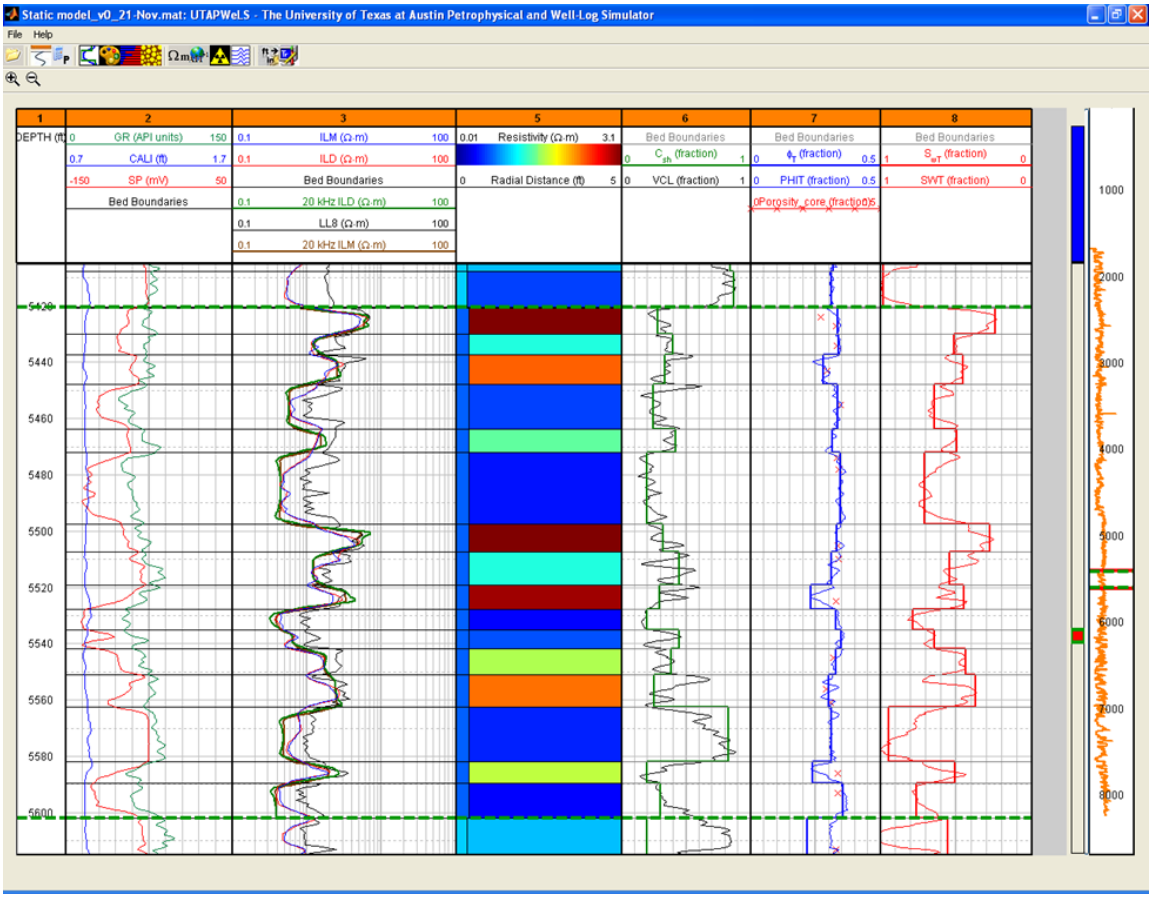

Figure 36. Result of the static model simulation in UTAPWeLS® for the ILD and ILM curves

Dynamic modeling: A finite difference grid was used in the simulation of mud-filtrate invasion and array induction measurements. Figure 6 shows the result of the first iteration of the dynamic model for the initial guesses of permeability values from the static analysis. A grid of 31 radial blocks and 36 vertical blocks was defined for the invasion simulation for a wellbore radius of 0.8 ft. The right three tracks display the C_{sh},

ϕ_t and S_w from the petrophysical characterization using IP®. The second track from the left shows the resistivity logging ILD overlapping with the results of the formation resistivity from the Earth Model. The first track to the left shows the GR, SP, and CALI data from wireline logs (Figure 37).

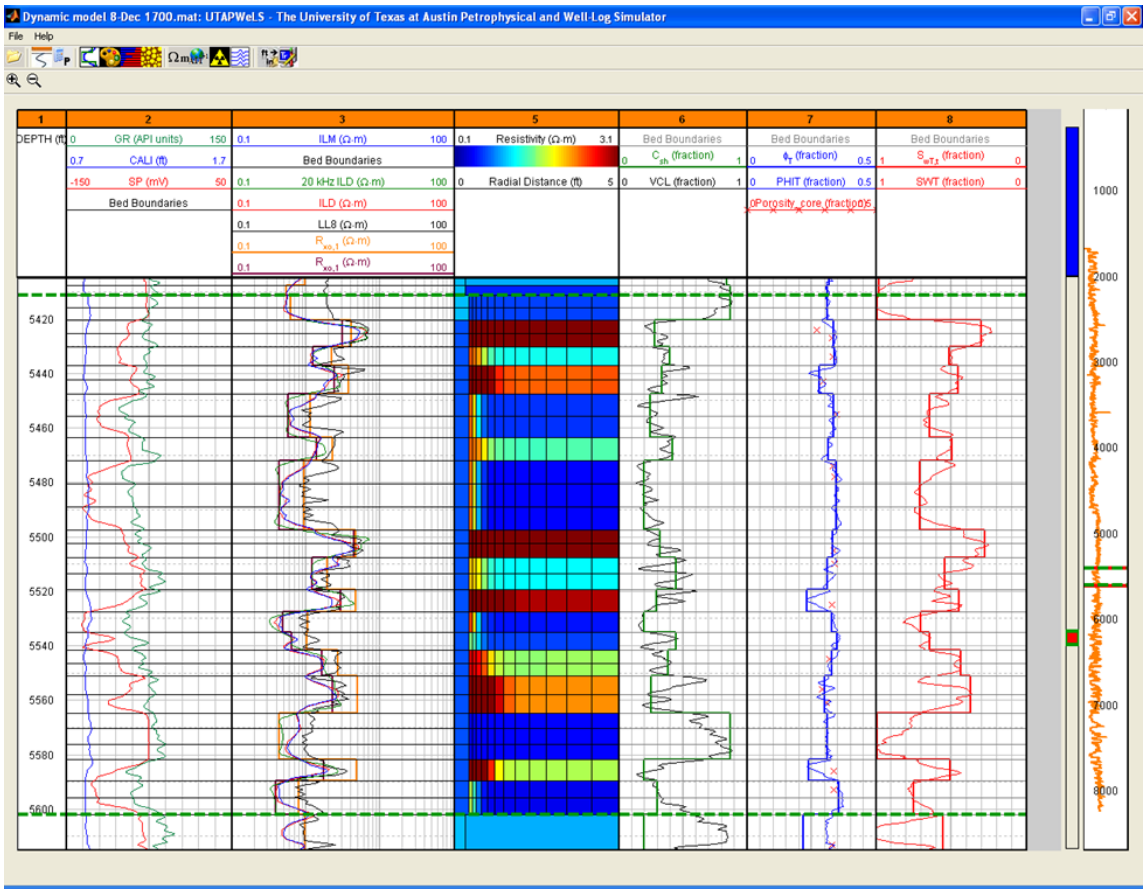

Figure 37. Result of the dynamic model simulation in UTAPWeLS®

According to the log header information, the logging operation was performed approximately 0.45 days after drilling. The results of the dynamic modeling for the radial distributions of pressure, salt concentration, resistivity, and water resistivity are shown in Figure 38. The maximum radius of invasion in the target zones A1 to A5 is about 2 ft;

this is due to the high porosity of the formation as they are inversely correlated. The fluid resistivity near the borehole (flushed zone) is very close to the mud filtrate resistivity of about 0.9 ohm-m at formation temperature. As the radius of invasion approaches the maximum, the fluid resistivity converges to 0.03 ohm-m (this is equivalent to about 110,000 ppm at formation temperature). The main deduction from the radial analysis is the shallow depth of invasion, which is also reflected in the overlay between the ILD and ILM curves in the log. This implies that the invasion profile analysis, to infer permeability, will need to rely on the separation between the shallow LL8 curve (10 in or 0.8 ft depth of investigation) and the deep resistivity ILD (60 in or 5 ft depth of investigation).

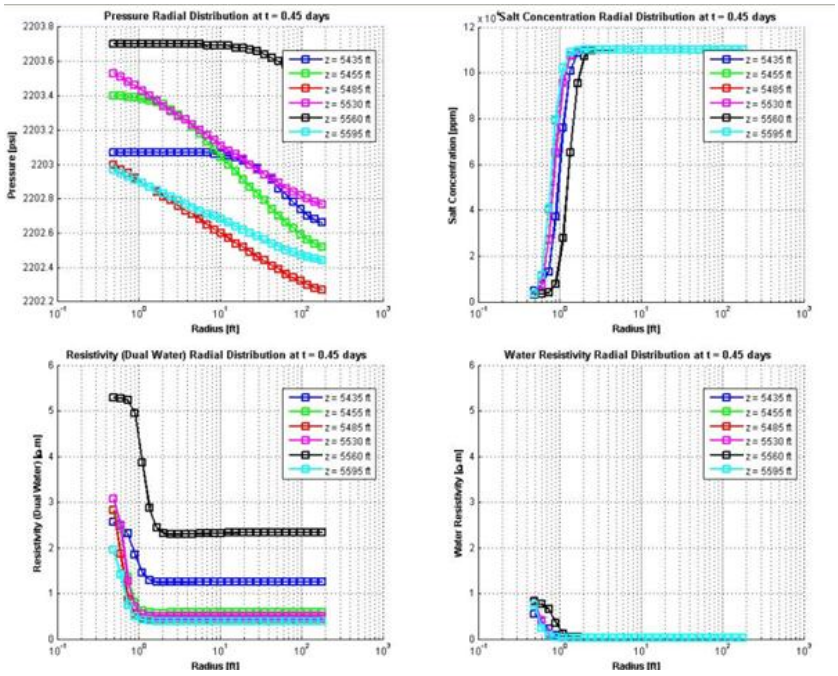

Figure 38. Pressure radial distribution at t = 0.45 days from drilling for the key well

Figure 39 shows the history of the invasion at 0.8 ft. The salt concentration undergoes a transition from reservoir conditions (about 110,000 ppm) to mud concentration levels (about 6,000 ppm). Due to the high permeability, the salt concentration reaches its minimum after about one day, meaning that is the time it takes for the formation at this radial depth to be completely flushed by mud.

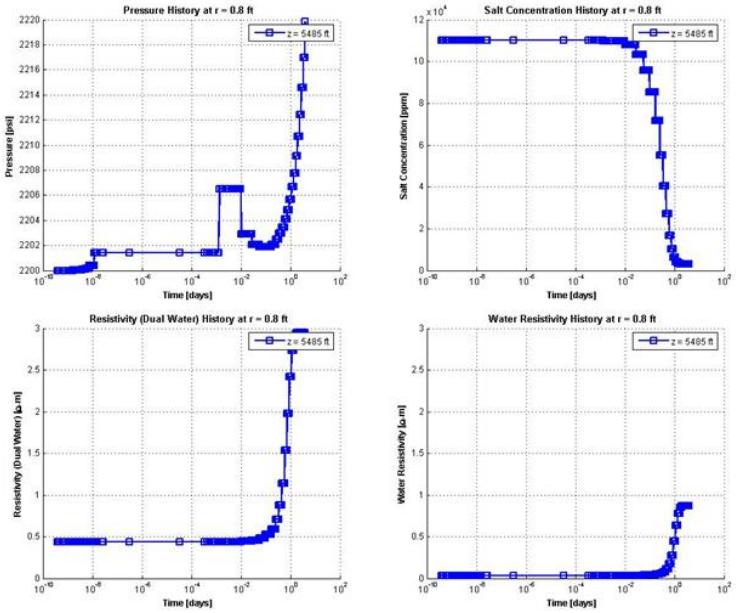

Figure 39. Invasion history for a radial depth of 0.8 ft for the key well

Estimation of absolute permeability: Having defined the rock characteristics (i.e. Brooks-Corey coefficients, total porosity, shale concentration) and the initial conditions (i.e. water saturation, water salinity) for all the petrophysical layers, a sensitivity analysis on permeability was performed. The objective is to adjust the value of permeability until there is an agreement between the resistivity curves ILD and LL8 from logs and the radial Zone 3 (0.8 ft) and Zone 10 (5 ft) resistivities from the invasion simulation. Brooks-Corey equations for different values of permeability were created. It

was assumed that all the layers (sands 1 to 5) share the same pore structure and, therefore, they also share the same Leverett J-function. Consequently, the P_c^o and e_p were recomputed for the reconstructed curve obtained from the equation

$$P_{cj} = P_{c1}\sqrt{\left(\frac{k_1}{\phi_1}\right)\left(\frac{\phi_j}{k_j}\right)}$$

where $k_1$and $\phi_1$are the values available from the core analysis and k_j and ϕ_j the values of k and ϕ of the new hypothetical curve to be generated. In this particular case, the value of ϕ is known with a good degree of accuracy and is practically the same for all the sands A1 to A5. Consequently, this equation is simplified to:

$$P_{cj} = P_{c1}\sqrt{\left(\frac{k_1}{k_j}\right)}$$

The result of the sensitivity analysis for k is shown in Figure 40. The values of resistivity in most of the sands are sensitive to only very low values of permeability (below 1 md approximately). This result does not allow us to take any conclusion about the permeability of these formations since we know from core analysis that they vary in the range of 100-2500 md. In order to verify these results, a similar analysis was performed for a second key well (key well 2).

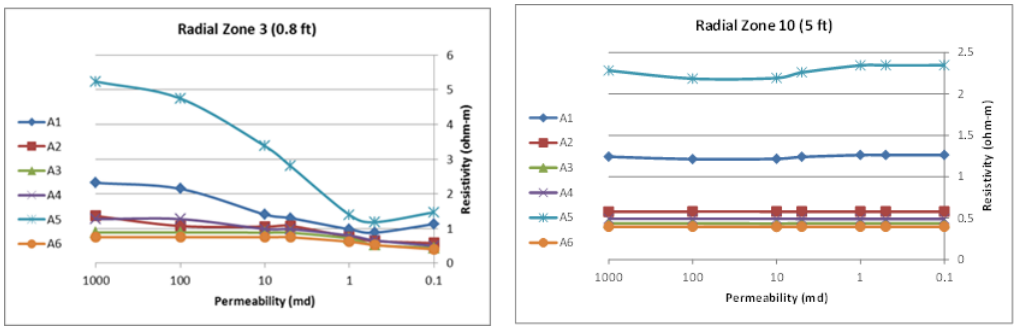

Figure 40. Results of the sensitivity analysis on absolute permeability for the key well

Invasion modeling analysis for key well 2: The petrophysical zones defined for this well take into account the results of the Lorentz plot analysis for key well 1. This means there are no major flow sub-units within the sands of interest assuming they have similar pore size characteristics. A static model was created taking as input the values of Csh, Sw, and ϕ from IP® analysis. The results from the simulation are shown in Figure 24. Log header information suggests that the log was acquired about 0.3 days after drilling. The results of the dynamic modeling for 0.3 days of invasion exhibit a good match with the resistivity curves at 10 in (0.8 ft) and 20 in (1.7 ft) or Radial Zones 3 and 7 respectively.

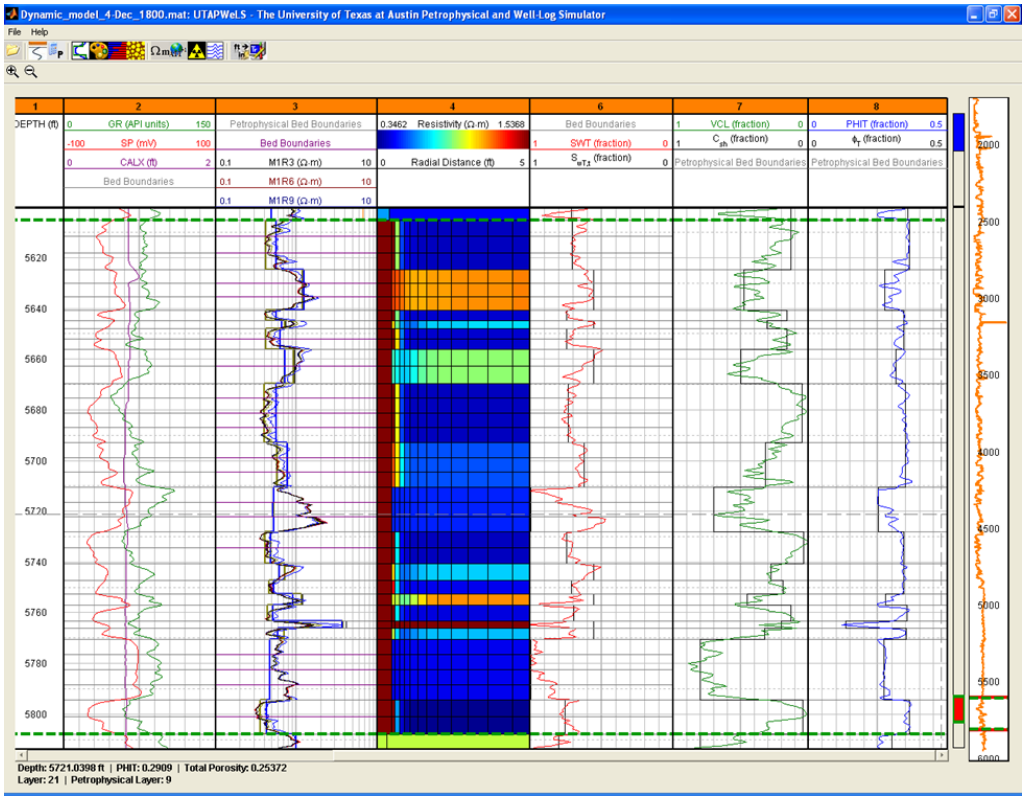

Figure 41. Result of the dynamic model simulation in UTAPWeLS® for key well 2

A grid of 31 radial blocks and 34 vertical blocks was defined for the invasion simulation for a wellbore radius of 0.4 ft (Figure 41). The right three tracks display the $C_{s\square}$, ϕ_t and S_w from the petrophysical characterization using IP®. The second track from the left shows the resistivity values M1R1 (10 in depth of investigation) and M1R2 (20 in depth of investigation) overlapping with the results of the dynamic simulation. The first track to the left shows the GR, SP, and Caliper data from wireline logs.

Figure 42 shows the radial distribution at 0.3 days of invasion. The maximum radius of invasion is about 1.5 ft, which supports the fact that all the resistivity curves' 30, 60, 90, and 120 in. depth of investigation are overlaying at formation resistivity values. Unfortunately this means only two out of five resistivity curves, M1R1 and M1R2 with depths of investigation of 10 in and 20 in respectively, will be available to assess the variability of the permeability. The resistivity curves M1R1, M1R2, M1R3, M1R6, M1R9 and M1RX are all outputs of the HIDL (Mark of Baker Hughes) tool.

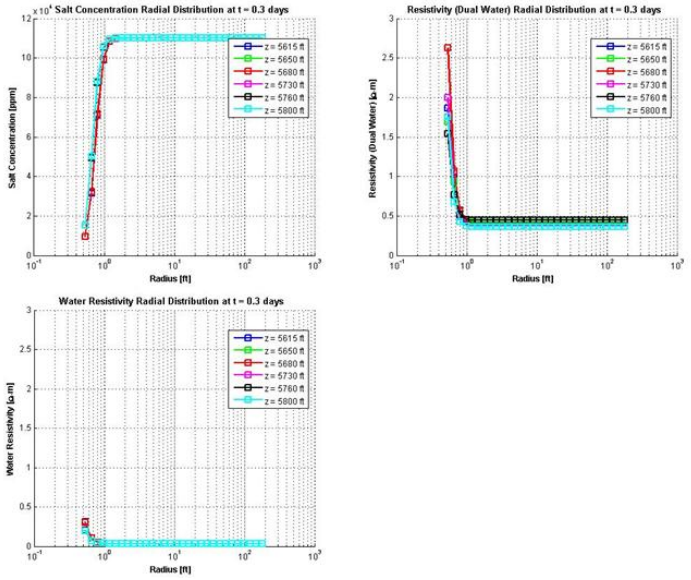

Figure 42. Pressure radial distribution at t = 0.3 days from drilling for key well 2

Figure 43 shows the behavior of the invasion for the Radial Zone 3 at 0.8 ft depth of investigation. In line with the previous analysis for key well 1, the formation at this depth is completely flushed with mud approximately 1 day after invasion starts.

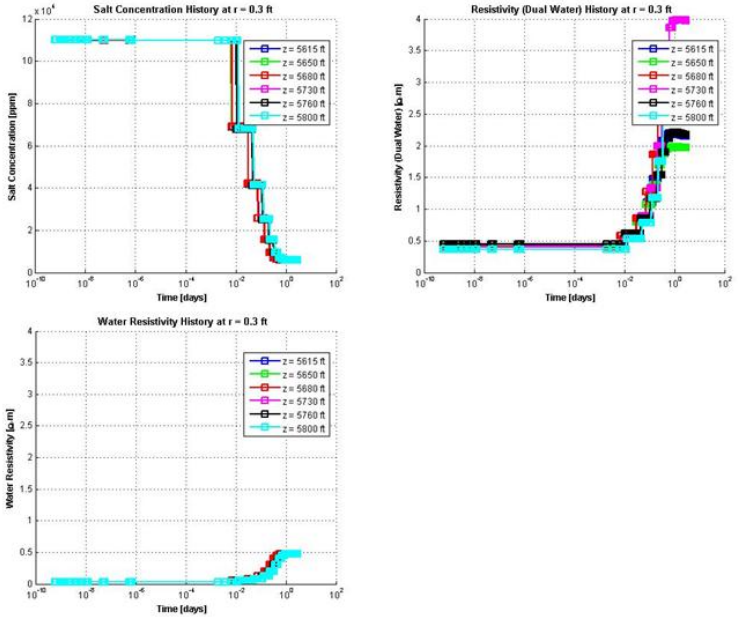

Figure 43. Invasion history for a radial depth of 0.8 ft for key well 2

A sensitivity analysis was performed in the same fashion as key well 1. The results are shown in Figure 44. Unfortunately the results are very similar, and the invasion model is sensitive only to values lower than about 1 md for the Radial Zone 3. Since the Radial Zone 7 is almost the same as the maximum radius of invasion (1.7 ft), the effect of changing the permeability values is negligible.

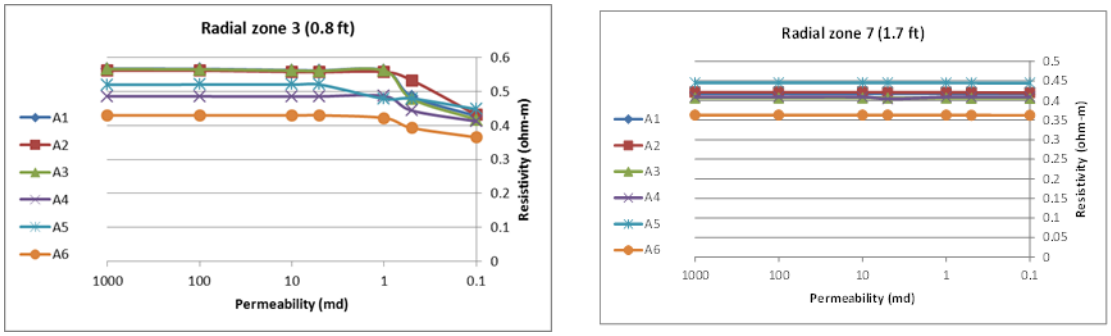

Figure 44. Results of the sensitivity analysis on absolute permeability for key well 2

From the previous analysis for key wells 1 and 2 it can be concluded that:

- The maximum radius of invasion in the production units A1 to A5 is very small (1.5 to 2 ft) due to the high porosity of the formation. The low radius of invasion limits the contrast between resistivity curves at different depths of invasion so only the shallow ones (and ones more affected by borehole effects) are useful for the invasion analysis.
- The rate of invasion is very high; consequently, the transition zone is entirely flushed about one day after invasion starts. Due to this rapid change in salinity during the invasion process, the time when the log was acquired (from the time when drilling occurred) needs to be known with a good degree of accuracy.
- The model is not sensitive to values of permeability higher than about 10 md, which does not allow for obtaining any permeability estimate for the injection zones. It is believed that this is a combined result of several factors
    - The low radius of invasion makes the deep resistivity curves unperturbed by the mud and therefore insensitive to any change of permeability
    - The high rate of invasion at relatively high values of permeability (>10 md) makes the mudcake form rather quickly and the invasion stop in about one day after drilling. Under this scenario, it is more critical to know the time

when the logs were acquired since the change in resistivity is affected dramatically by time

- At high values of water saturation (close to irreducible in this scenario), the capillary pressure is very small, making the effect of permeability almost negligible for relatively high values of permeability

Accuracy estimation: The previous results do not allow the inference of any better permeability data compared to the empirical SP regression, but they agree with previous studies of permeability data from resistivity logs that suggest that at high water saturations the accuracy of resistivity measurements become more significant for correct permeability results (Saner, 1997). This study in particular suggests that permeability estimation from resistivity data is more accurate for low-permeability (0.01 to 100 md) samples. The methodology described in this publication was not applied in this study since the value of water saturation was unknown by the time the resistivity logs were acquired.

A successful study (Salazar et al., 2005) performed in tight gas sands ($k < 1$ md) shows a 75% agreement between core data and estimated permeability from invasion modeling using UTAPWeLS®. Since Company A has around 70 wells available for logging/coring, the total accuracy, taking into account the geostatistical spatial accuracy, is estimated as $0.75 \times 0.834 \cong 0.60$. The inferential analysis for UTAPWeLS® analysis will use an accuracy of 0.60 for the VOII quantification.

2.2.10 Value of Information from UTAPWeLS® Analysis

2.2.10.1 Inferential analysis for imperfect information

The decision tree in assessed and inferential forms, after performing Bayesian inference representing the information and uncertainties in the UTAPWeLS® scenario, is

shown in Figure 45. Note that p(Si) = p("Si") which agrees with the previous assumption that the reservoir modeling is 100% accurate. By improving the quality of the information-gathering activity, the likelihood of each scenario "Rj" is increased, but the preposterior probabilities remain equal to the priors.

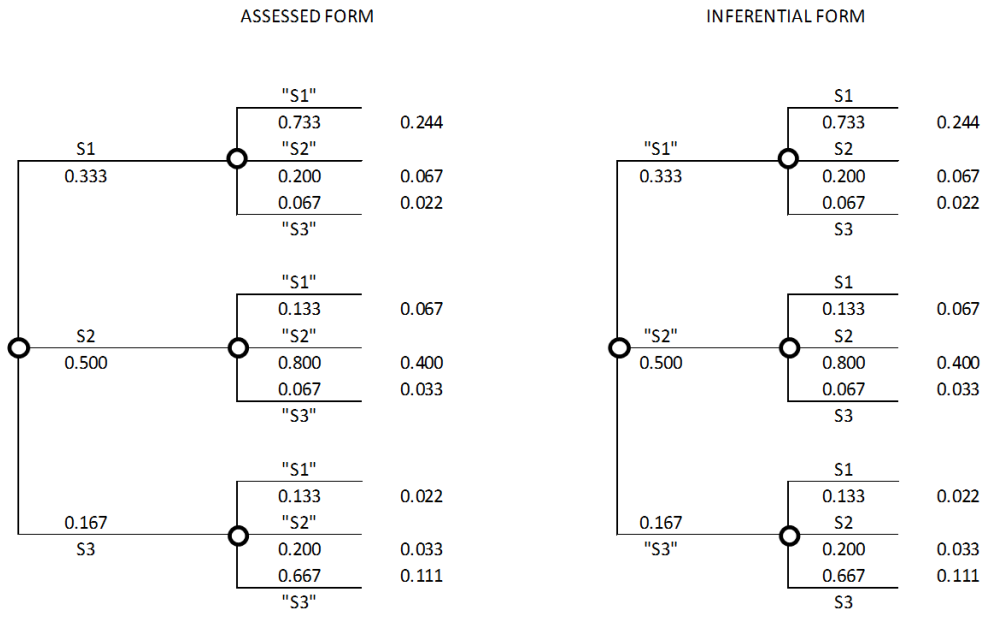

Figure 45. Decision tree in assessed and inferential forms representing the information and uncertainties for UTAPWeLS® methodology

2.2.10.2 Quantification of VOII for UTAPWeLS® data

If it decides to acquire or develop a certain information-gathering methodology (in this case UTAPWeLS)®, Company A will have the option of signing or refusing the contract after observing the result of the test (report). The decision tree showing this scenario is illustrated by Figure 46. The conditional and marginal probabilities $p(S_i|"S_j")$ and $p("S_i")$ respectively are obtained from the decision tree in inferential form. The outcomes for all the possible scenarios "S_i" are the respective NPV_i defined previously in

section 2.1. It is assumed that the cost of performing the UTAPWeLS® study for the 75 wells with log information is approximately $100,000, corresponding with the time that a petro-technical professional or researcher would spend analyzing the data. The VOII in this case is equal to the Certain Equivalent with free information since the Certain Equivalent without information is zero as stated previously in section 2.2.5.

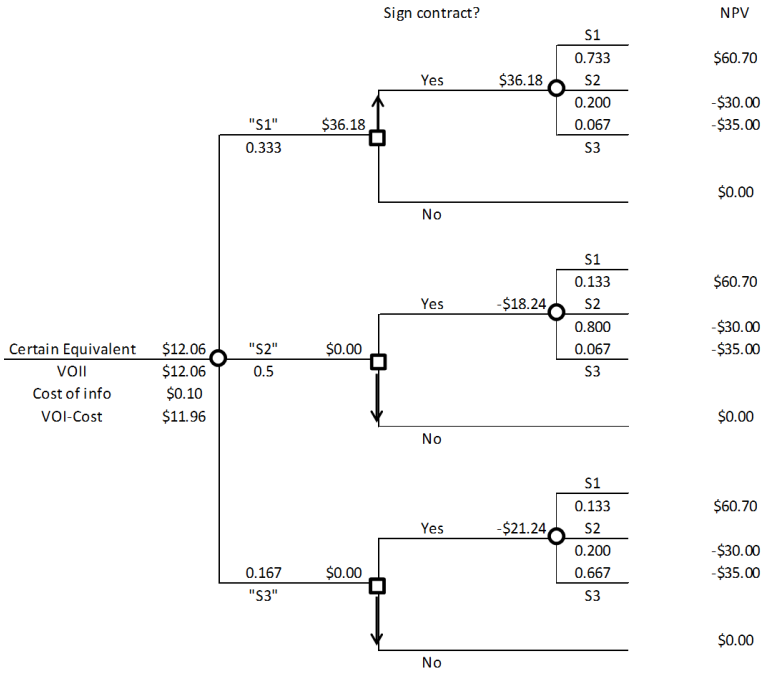

Figure 46. Decision tree showing the decision faced by Company A with additional information from UTAPWeLS® analysis

From the previous figure it can be inferred that Company A should pay for the UTAPWeLS® study, which is worth (VOII – costs) about $12 million under contractual requirements. If the test suggests that scenarios S2 or S3 will happen, then Company A should not sign the contract otherwise it is expected that losses will be incurred. If the test suggests that S1 will occur, Company A should agree to the contract, which will allow it to obtain a positive NPV1 directly proportional to the price of Carbon Credits ($/Ton).

The VOII is high due to the relatively good accuracy of the report compared to its low cost.

2.2.11 Value of Information from acquisition of new core/logging data

2.2.11.1 Inferential analysis for imperfect information

From the previous geostatistical analysis, the accuracy or goodness of fit of a core/logging-data-type of information-gathering will depend on the number of wells cored or logged. A Gaussian curve was fitted to the data points and be expressed as,

$$G = 1 - e^{\frac{-0.557\, n^2}{39^2}}$$

The decision tree in assessed and inferential forms after performing Bayesian inference representing the information and uncertainties for an accuracy G corresponding to logging 50 new wells is shown in Figure 47. For practical purposes and since coring/logging is a direct physical measurement of permeability, it is assumed that its accuracy is 100%

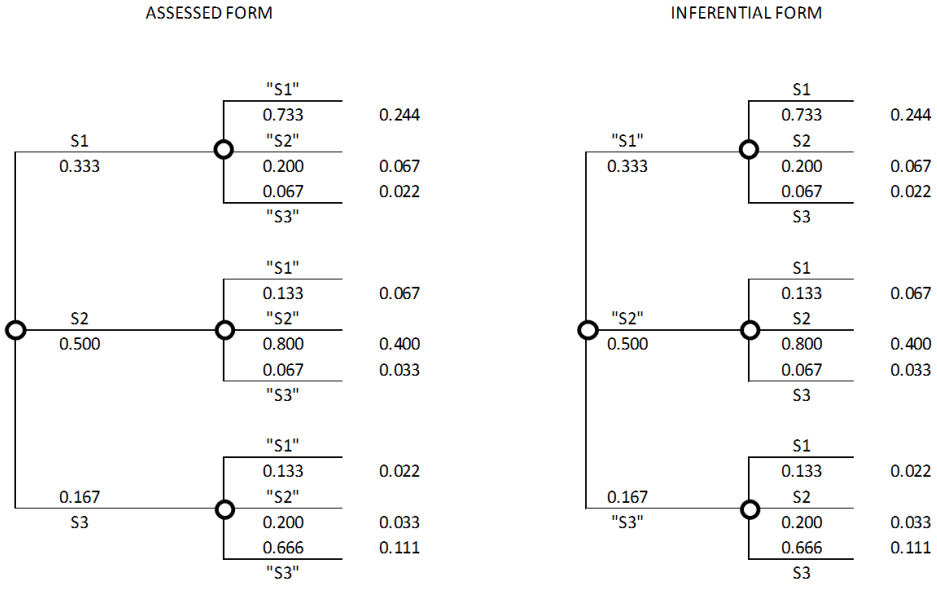

Figure 47. Decision tree in assessed and inferential forms representing the information and uncertainties for logging 50 wells

2.2.11.2 Quantification of VOII for new logged permeability data

The accuracy of the information-gathering activity will depend on the number of wells logged or cored. Typically the larger the number of wells logged, the more accurate the permeability map (Kravchenko, 2003). However, the cost of such tests can quickly exceed any potential benefits in the decision making process. Therefore, when choosing the optimal number of tests to be performed (wells), the number of tests should be balanced with the sampling costs. Based on estimates from oilfield services companies, it will be assumed that the cost of logging/coring each well is $200,000.

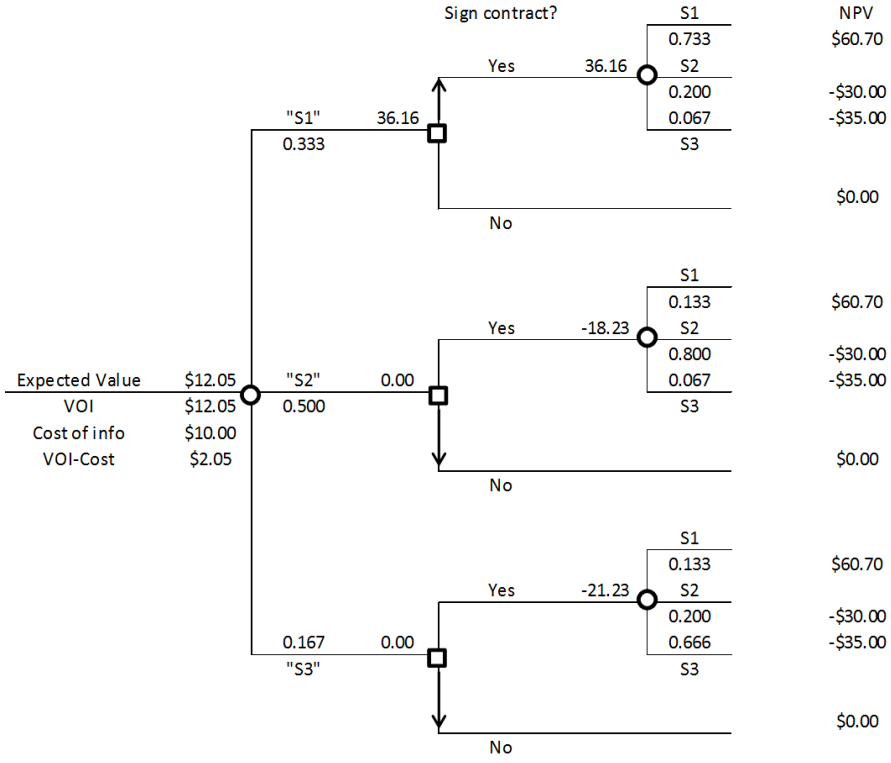

Figure 48. Decision tree for the deal with additional information from core/logging

Figure 48 illustrates the decision tree for the deal with additional information for an accuracy G = 0.600 (50 wells). Similar to the previous results from UTAPWeLS®,

whenever the test report suggests that scenarios S2 or S3 will happen, Company A should not sign the contract otherwise it is expected that losses will be incurred. If the test suggests that S1 will occur, Company A should agree to the project, in which case it will obtain a positive NPV1 directly proportional to the price of Carbon Credits ($/Ton). Recall from previous analysis that:

$$p("S_i"|S_i) = G + p(S_i)(1 - G)$$

$$p("\neg S_i"|S_i) = p(\neg S_i)(1 - G)$$

Figure 49 shows a superposition of the VOI of getting new information and logging acquisition costs as function of the number of wells. The cost of acquiring new data is a linear function depending on the number of wells logged/cored. It can be observed that at low numbers of wells logged/cored, the accuracy is not enough for the data acquired to be worthwhile. At some point the added value due to an increase in accuracy by logging new wells is high enough to overcome the associated costs.

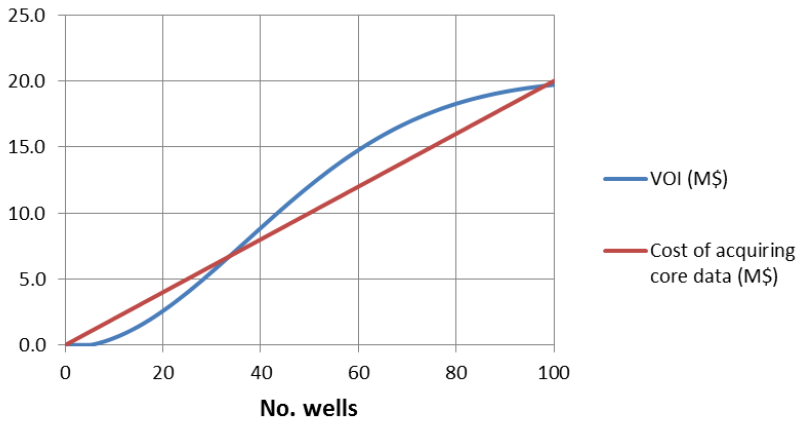

Figure 49. VOI and cost of acquiring data in function of number of wells cored/logged

The accuracy curve has an asymptotic behavior; at some point logging new wells will not add net value, and, consequently, the VOI will start decreasing until it reaches negative values (Figure 50). The optimum number of wells to be logged/cored under current conditions (contractual requirements) is 66 wells, where the net value of new acquired data (VOII – costs) is about $2.9 million. Regardless of budgetary constraints, all the wells are suitable for data acquisition; the minimum amount of wells to be logged for the data to be worthy (Net VOII > $0) is 34.

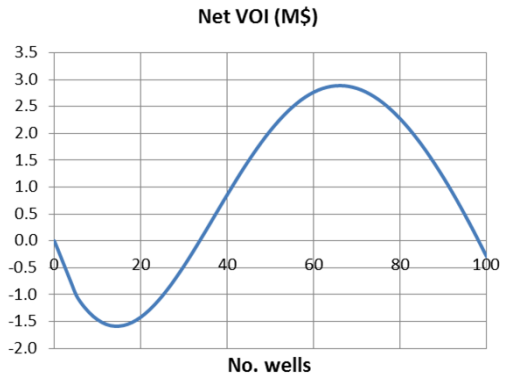

Figure 50. Net VOI (VOI – cost) in function of the number of wells logged/cored

Chapter 3. SENSITIVITY ANALYSIS

In previous chapters it was concluded that under the current contractual requirements (16.43 $/Ton CO2, 4 MTon of injection capacity and $30 Million contractual penalty fee), the Net VOII from UTAPWeLS® was about $12 Million, mainly due to the relatively good accuracy and low costs. The VOII for new cored/logged permeability data has a better accuracy compared to UTAPWeLS® methodology, but its costs are much higher. For that reason, the Net VOII was about $2.3 Million for an optimal number of 66 wells logged/cored. This chapter will explore the consequences of changing conditions in the contract that could potentially render the VOI to be worthless.

3.1 VOI SENSITIVITY TO CARBON CREDIT

The net carbon credit prices used to compute the VOI for different information-gathering activities available to Company A was $16.43 $/Ton. However, this is just an estimate as market conditions and associated costs could vary or the contract could be renegotiated. Figure 51 illustrates the variation of VOI with carbon credit values for different accuracies. Again, the VOI represents the maximum amount that Company A should be willing to pay for new data. Some observations can be inferred from this graph:

- For relatively low values of accuracy (e.g. 0.2 and 0.4) and carbon credit prices the VOI is worthless. This is due to the fact that the contract is so unfavorable that the test is not reliable enough to impact the decisions made by Company A. Therefore the VOI is zero.
- The VOI increases steeply with carbon credit prices until it reaches a maximum. This occurs because for carbon credit prices below the break-even value, the deal with no additional information is $0. Since VOI = CE with additional information -

CE with no information, any increase of CE with additional information is a net increase in the VOI.

- The VOI reaches its maximum when the deal with no additional information is profitable by itself (CE > $0). The point of maximum VOI represents the break-even carbon credit price (Delquié, 2008). The VOI starts decreasing as the CE with no information is now a positive value being deducted from the CE with additional information.
- At certain relatively high values of carbon credit the VOI become worthless again; at this point no matter what the result of the test is, Company A will proceed by signing the contract. As stated earlier, if the result of a particular test does not affect the decision, then the value of that information is zero. At high values of carbon credit the deal with no information still has only a 0.333 probability of success (prior probability of S1). However, if perfect information is available, the DM will have a 100% chance of success if the test suggests that S1 will occur (zero risk). At values of carbon credit higher than 20 $/Ton, the increase in expected value for the deal with no information and additional information is the same; therefore the net VOPI is zero and the curve's plateau is at $20.8 million.

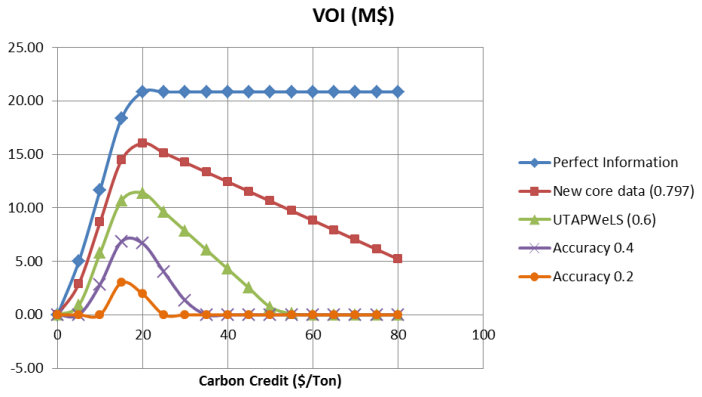

Figure 51. Variation of VOI with Carbon Credit for different accuracy values

Equivalent results in a different format for carbon credit prices higher and lower than the break-even value are shown in Figures 52 and 53. Note that, for any value of accuracy, the VOI is maximum at the break-even carbon credit price of 16.875 $/Ton. In line with previous remarks (Delquié, 2008) related to intensity of preference, it is clear that the VOI is maximum when the DM is indifferent between the option of refusing the contract or signing it with a contractual fixed price of 16.875 $/Ton.

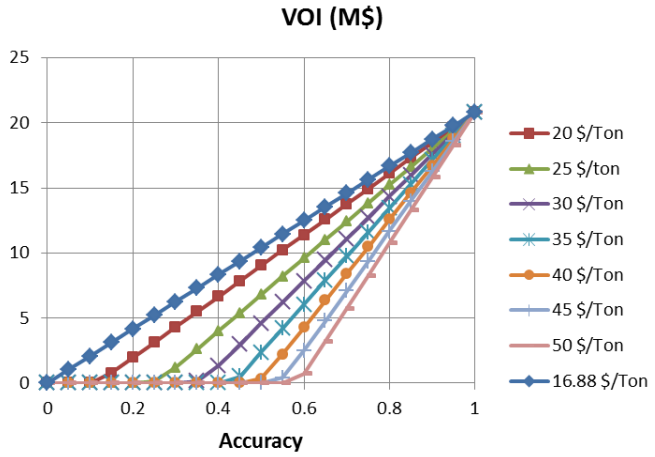

Figure 52. Variation of VOI with accuracy for different carbon credit values higher than the break even carbon credit price

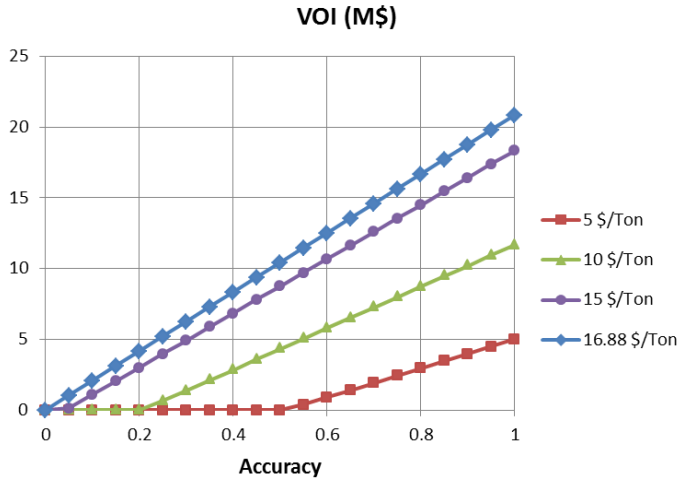

Figure 53. Variation of VOI with accuracy for different carbon credit values lower than the break even carbon credit price

3.2 VOI SENSITIVITY TO STORAGE CAPACITY CONTRACTUAL REQUIREMENT

Figure 54 illustrates the variation of VOI with the contractual storage requirement for different accuracies. Similar to the previous line of reasoning, the curves reach a maximum when the projects become economically feasible with no additional information. The graph shows that, provided the reservoir can handle larger amounts of CO2, there is a window of values of storage capacity in which the VOI has some value that is higher as accuracy improves. Outside of this window the VOI is worthless because the test does not change Company A's decision to proceed or not with the contract based on prior probabilities. Consistent with previous results, the VOPI plateaus at $20.83 million at about 4.2 MTon of CO2. Note that for the current scenario of 4 MTon of CO2, the VOPI is $20.23, which is consistent with previous results.

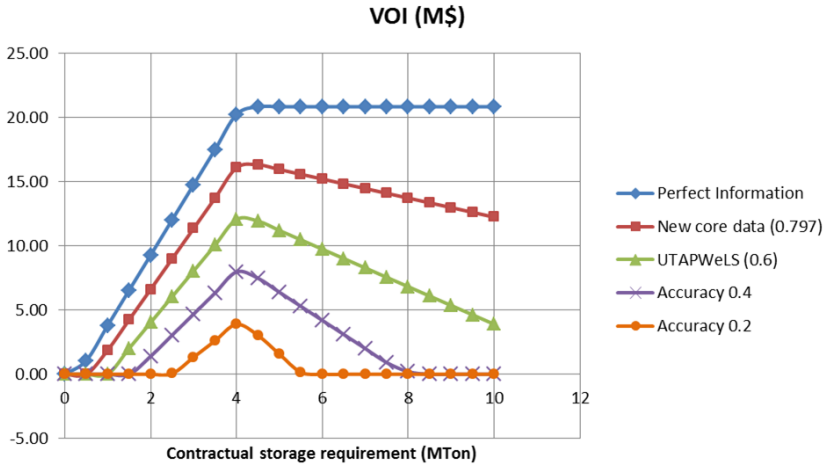

Figure 54. Variation of VOI with contractual storage requirement (MTon) for different accuracies

3.3 VOI Sensitivity to cost of acquiring new data via logging/coring for unlimited number of wells and unconstrained budget

Let us assume that it is possible for Company A to use all the existing wells in the field of interest (approximately 80 wells), and there is no budgetary constraint on the amount of money to be spent on the information-gathering activity (provided it adds value to the project). Under current contractual requirements and the cost of acquiring new core/logging data at $200,000 per well, the Net VOI of such an information-gathering exercise is around $2.9 million (Figure 55). However, it can be noted that should the carbon credit be lower (let us assume 12.5 $/Ton), the information is worthless as the cost of acquiring the data exceeds the benefit to the decision making process. This Net VOI is represented by the maximum positive gap between the cost and expected value in Figure 49 for each scenario of carbon credit price.

For example, under the scenario 17.5 $/Ton, the company should not be willing to pay more than about $250,000 per well for acquiring new data. However, if the logging/coring provider is willing to renegotiate the terms of the contract and/or Company B is willing to renegotiate the carbon credit amount, Figure 55 gives an estimate of the maximum amount Company A should be willing to pay for the log/core services. The number of wells is optimized to obtain the maximum gap between expected value and acquisition costs in Figure 49 assuming that all the wells available for acquiring new information allows for such flexibility.

It can also be noted that at carbon credit prices of about 20 $/Ton, the trend of the graph tends to go backwards. In other words, the graph trends back towards the origin which is consistent with the previous result in Figure 51 where the VOI was maximum at values of about 20 $/Ton.

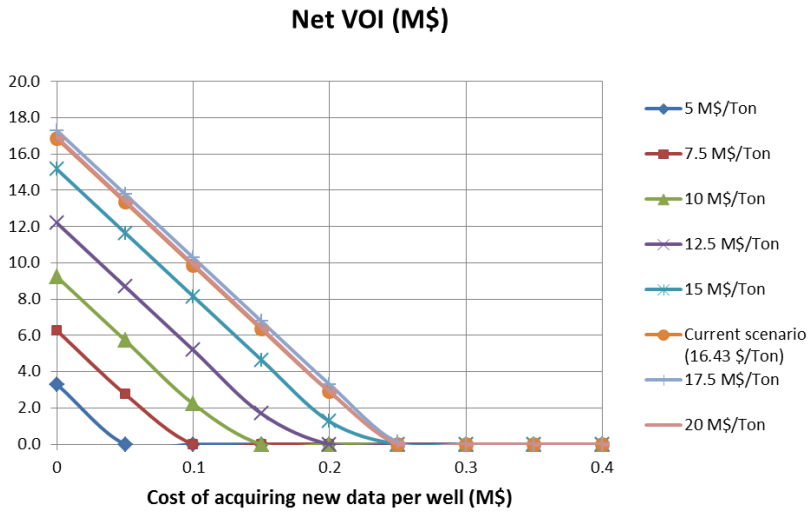

Figure 55. Net VOI for acquisition of new data in terms of carbon credit prices and cost of acquiring new data

Figure 56 is a similar graph for higher (but unrealistic) values of carbon credit. The Net VOI curves are much closer to each other, which is also consistent with the results from Figure 51 where the VOI decreases slowly for carbon credit values higher than the break-even price.

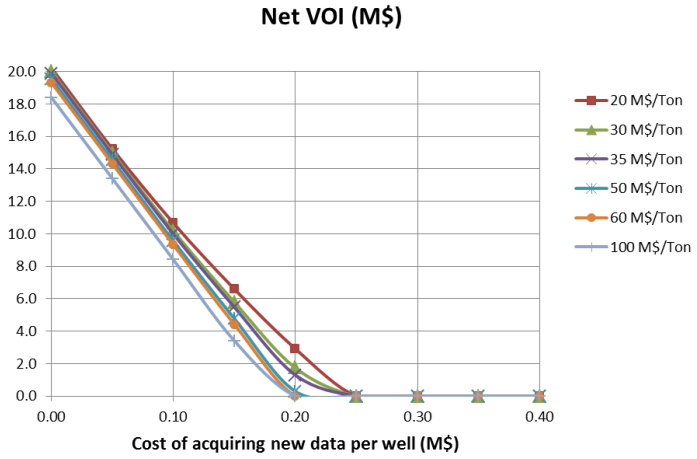

Figure 56. Net VOI for acquisition of new data in terms of carbon credit prices and cost of acquiring new data

3.4 VOI SENSITIVITY TO COST OF ACQUIRING NEW DATA VIA LOGGING/CORING FOR LIMITED NUMBER OF WELLS OR CONSTRAINED BUDGET

Let us assume that Company A has the budget constraint and/or accessibility issues that make it possible to log/core only 20 wells. According to the results in Figure 50, the net VOI will be the difference between the Expected Value with additional information and the cost of acquiring such information, which is negative (-$1.41 million) for the current scenario ($200,000 per well logged/cored). However, it is possible for Company A to negotiate the contract with the log service provider in order to make such information-gathering worthwhile. The question is, what is the maximum amount that company A should be willing to pay per well cored/logged?

Figure 57 shows a sensitivity analysis of the cost of acquiring new data (M$) versus Net VOI for different well configurations. Note that, for 20 wells, Company A should not be willing to pay more than $120,000 per well logged/cored, otherwise there is no benefit from the information-gathering activity.

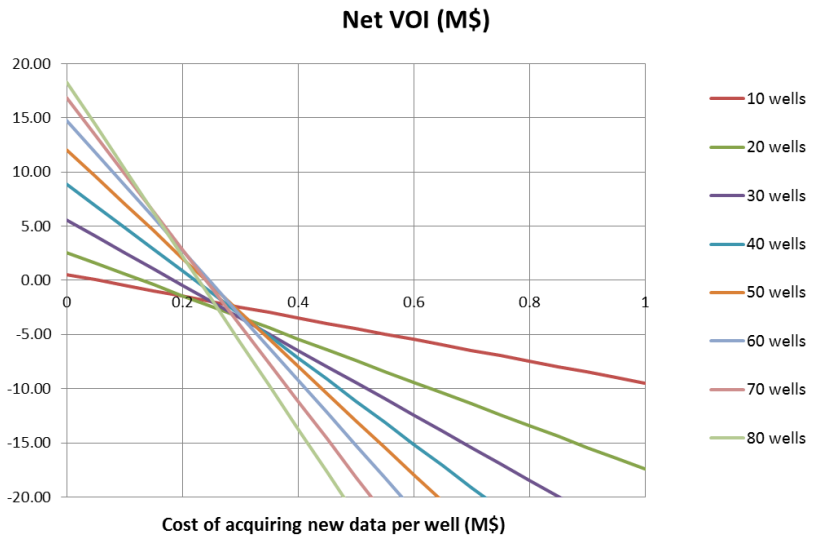

Figure 57. Sensitivity analysis of cost of acquiring new data (M$) versus Net VOI for different well configurations

3.5 VOI SENSITIVITY TO ACCURACY OF RESERVOIR MODELING

In order to capture the true value of permeability assessment tests, the previous results in this report assumed that the outcomes "Si" of the reservoir modeling describe the state of nature with 100% confidence based on certain permeability distribution Ri. By relaxing this assumption and defining "M" as the reservoir modeling accuracy, the following can be inferred by applying a similar reasoning to section 2.2.6,

$$p("S_i"|S_i) = G\ M + p(S_i)(1 - G)$$

$$p("\neg S_i"|S_i) = p(\neg S_i)(1 - G) + \frac{(1 - M)}{(n - 1)}$$

where n = $No.of\ S_i\ realizations$

A common way of handling non-informative probabilities is following the principle of insufficient reason (Gilbert et al., 2008). Consequently, the previous equations assume that if the reservoir modeling fails to predict the real state of nature Si, the remaining probability $p("\neg S_i"|S_i)$ (or specificity) will be distributed uniformly (all events are equally likely) among the rest of "$\neg S_i$ realizations.

The decision tree in assessed and inferential forms for an accuracy M = 0.8 and G = 0.6 (UTAPWeLS® methodology) is shown in Figure 58. Note that the prior and pre-posterior probabilities are now different as p(Si) ≠ p("Si") when M ≠ 1.

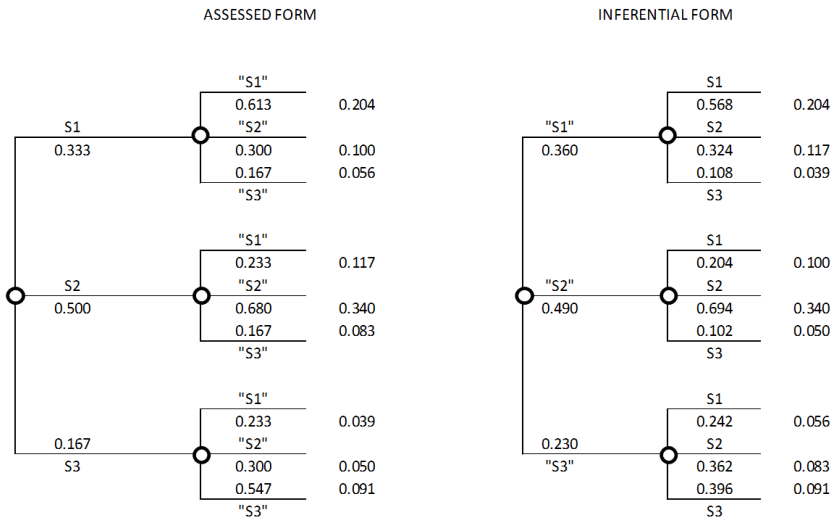

Figure 58. Decision tree in assessed and inferential forms for a reservoir model with accuracy M = 0.8 and G = 0.6 (UTAPWeLS® accuracy)

Figure 59 illustrates the VOI for different values of accuracy G and M. Note that when G = 1.0 (hypothetical scenario with many data points in the field), the VOI is zero at M = 1/3, which is equivalent to assuming a uniform distribution among the three realizations S1, S2 and S3. When the two tests are perfect (G = 1.0 and M = 1.0) the VOI reaches it maximum value at VOPI = $20.23 million, which is in agreement with previous results.

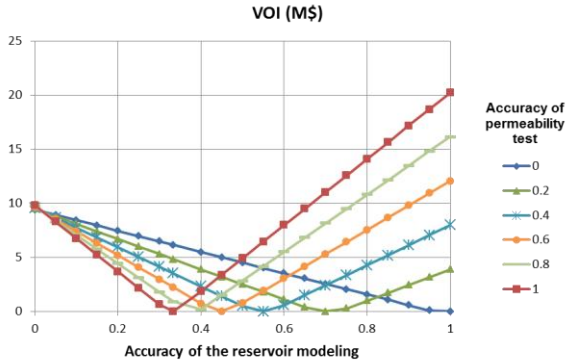

Figure 59. VOI for different values of accuracy G (permeability tests) and M (reservoir modeling)

3.6 SUMMARY

Based on the prior knowledge about the reservoir, a decision analysis framework was set up in order to estimate the VOI of acquiring new permeability data. The VOI represents the maximum amount that a DM should be willing to pay for certain information-gathering activites. A geostatistical analysis implemented with SGeMS® software was used to bridge local (punctual) accuracies, distributed spatially over the field of interest (Block B), to the accuracy of the inputs for a reservoir model developed in GEMS® software.

The UTAPWeLS® model applied to Block B is not useful to infer permeability data under the current petrophysical characteristics of the reservoir, specifically regarding capillary pressure and relative permeability curve profiles. An estimated accuracy for this methodology based on an application in a different field was used for illustration of VOI quantification. Permeability tests (like physical coring or DST operations) posed a better accuracy compared to the numerical-based UTAPWeLS® methodology. However, once the costs of acquiring the information are considered, the lower accuracy method proved to be more valuable to the project.

Sensitivity analysis showed that Bayesian inferential analysis can be used to optimize the number of wells to be tested in order to maximize the VOI. It is also possible to estimate what variable(s) in the contract can be modified to increase or maximize the VOI and the intervals in which the VOI is worthwhile for the main parameters in the contract: carbon credit price ($/Ton of CO2), penalty fees for not meeting storage contractual requirements ($), and cost of buying new land to meet regulatory requirements ($).

Chapter 4. CONCLUSIONS AND FINAL CONSIDERATIONS

4.1 CONCLUSIONS

Under the assumption of risk neutrality (Howard, 2005) and with the current state of information, the CCS project faced by Company A is not economically feasible due to the combination of several factors, specifically carbon credit prices, penalty fees, and probability of not meeting contractual requirements.

Out of the three information-gathering activities available to Company A, namely UTAPWeLS® analysis, drilling new wells, and acquiring new data by logging/coring existing wells, only the last of these is feasible. UTAPWeLS® did not render valid results due to a combination of several petrophysical properties. At the same time, drilling enough wells to achieve a minimal degree of accuracy for the degree of heterogeneity of the reservoir (i.e. accuracy values for which VOI > 0) would become extremely expensive for the scale of the project. Fortunately, Block B is a long-standing oil field with high well density, and Company A has the advantage of using these locations to acquire permeability data sets (provided those wells are accessible for logging operations). The geostatistical analysis showed that, for the number of wells available for testing (DST's or coring/logging) in the field (70 wells), it is possible to obtain a significant estimation of the permeability distribution in the reservoir.

If Company A has limited availability of wells for logging operations or a limited budget, it is still possible to optimize the number of locations tested by maximizing the VOI of newly acquired permeability data. If the wells available for logging and/or the budget are not enough to reach a minimal degree of accuracy (i.e. accuracy values for which VOI > 0), Company A could still renegotiate the costs of data acquisition with the service provider (e.g Oilfield Service Company) to a minimum value that would make the newly acquired information worthwhile.

If none of the options mentioned above are available, Company A would have to modify some of the contractual requirements. For example, the project can become profitable with no additional information by changing the prior probabilities of the different scenarios S1, S2 and S3. In fact, by increasing the length of the contract from three to four years (until 2018) for the same amount of injected CO2 and penalty fees, the prior probability for S1 increases, making the Certain Equivalent of the project (with no additional information) positive, and perhaps high enough that any additional information is worthless.

4.2 FUTURE WORK

Future work might do further research in the following scenarios:

1. Prior probabilities for scenarios S1, S2, and S3 were based on discrete permeability probability distributions (R1, R2,…,R12). Future work could implement a design of experimental approach that expresses the expected outcome of a realization as a function of expected permeability distributions. A Bayesian inference for continuous probability distributions in a decision-tree framework might not be convenient under this scenario.
2. Detailed geostatistical analysis taking into account 3D variability and higher number of Gaussian realizations in order to improve the estimation of spatial accuracy
3. Implementation of an EOR setup where oil/gas production affect the outcomes of the project with and without information. Under this scenario, the elevated pressure would be dissipated through the production wells, thus increasing the ability to inject more CO2 due to volume. In an EOR setting, the extent of the plume and storage capacity might not be sensitive to the permeability

distribution of the reservoir, in which case the VOI of permeability estimates should be negligible.

Bibliography

Agarwal A., Parsons, J., Commercial Structures for Integrated CCS-EOR Projects. Energy Procedia, Volume 4, 2011, Pages 5786–5793

Aggrey, G. H., Davies, D.R., Ajayi, A., Konoczynski, M. Data Richness and Reliability in Smart-Field management – Is There Value? Paper SPE 102867, September 2006, DOI: 10.2118/102867-MS

Ang, A., Hua, S. and W. H. Tang. Probability Concepts in Engineering: Emphasis on Applications in Civil and Environmental Engineering. New York: Wiley, 2007

Angus, S., Armstrong B., de Reuck K.M., 1973, International Thermodynamic Tables of the Fluid State Volume3. Carbon Dioxide. IUPAC Division of Physical Chemistry, Pergamon Press, London, pp. 266-359

Ballin, P. R., Ward, G. S., Whorlow, C. V., Kahn, T. Value of Information for a 4D-Seismic Acquisition Proejct. Paper SPE 94918. June 2005, DOI: 10.2118/94918-MS

Benson S.M., 2006, Monitoring Carbon Dioxide Sequestration in Deep Geological Formations for Inventory Verification and Carbon Credits, SPE 102833

Bickel, J. E., Gibson R. L., McVay D. A., Pickering S., Waggoner J. Quantifying the reliability and value of 3D land seismic. SPE Reservoir Evaluation & Engineering. Volume 11, Number 5. October 2008

Bock, B., Rhudy, R., Herzog H., Klett, M., Davison, J., De La Torre Ugarte, D. G., Simbeck D., Economic Evaluation of CO2 Storage and Sink Enhancement Options. Final Technical Report, February 2003

Branco, C. C. M., Pinto, A. C. C. Tinoco, P. M. B., Vieira, P. M. F., Sayd, A. M., Santos R. L. A., Prais F. The Role of the Value of Information and Long Horizontal Wells in the Appraisal and Development Studies of Brazilian Offshore Heavy-oil Reservoir. Paper SPE 97846, November 2005, DOI: 10.2118/98746-MS

Bratvold R. B., Bickel J. E., Lohne H. P., Value of Information in the Oil and Gas Industry: past Present and Future. SPE Reservoir Evaluation & Engineering, 2009. SPE 110378

Bryant E, Climate process and change. Cambridge, UK: Cambridge University Press; 1997. p. 209.

Burgess K.A., MacDougall T.D., Siegfried R.W., Wireline-Conveyed Through-Casing Formation Tester Preserves Casing Integrity. SPE 72371, October 2001

Celebi M., Graves F., January 2009. Volatile CO2 prices discourage investment. Harvard press

Coelho, A.C.D., De Camrgo C., Kato, E.T., Legrand V.M.Q.F., Utilizing Mini-DST for Formation Evaluation, SPE 94963, June 2005

Coopersmith, E. M., Burkholder, M. K., Schulze, J. H. Value-of-Information Lookbacks – Was the Information You Gathered Really Worth Getting? Paper SPE 101540, September 2006, DOI: 10.2118/101540-MS

Cressie N., Aldworth, J., Spatial Statistical Analysis and its Consequences for spatial sampling, E.Y. Baafi and N.A. Schofield editors, Geostatistics Wollongong 1996, Volume 1, 126-137

Davis, D., Scott, M., Roberson, K., Robinson, A., Large Scale CO2 Flood Begins Along Texas Gulf Coast, SPE 144961-MS, July 2011

Delquié, P. The Value of Information and Intensity of Preference. Decision Analysis Vol. 5 No. 3, 2008

Demirmen, F. Subsurface Appraisal: The Road From reservoir Uncertainty to Better Economics. Paper SPE 68603. April 2001, DOI: 10.2118/68603-MS

Demirmen, F. Use of "Value of Information" Concept in Justification and Ranking of Subsurface Appraisal. Paper SPE 36631, October 1996, DOI: 10.2118/36631-MS

Deutsch, C.V., Direct Assessment of Local Accuracy and Precision, E.Y. Baafi and N.A. Schofield editors, Geostatistics Wollongong 1996, Volume 1, 115-125

Dewan, J.T., 1983, Essentials of Modern Open-Hole Log Interpretation: PennWell Publishing Company

Ellis, D. V., Singer, J. M. Well Logging for Earth Scientists, Second Edition, Springer, 2008

Gilbert, Robert B., Min Namhong, and Larry W. Lake. A Sound Foundation for Assessing Probabilities. Austin: The University of Texas at Austin, 2008

Gotway C. A., Ferguson R. B., Hergert R. W., Peterson T. A., Comparison of Kriging and Inverse-Distance Methods for Mapping Soil Paramters, Soil Science Society of America Journal, 60: 1237-1247 (1996)

Gringarten, E., Deutsch, C, Teacher's Aide Variogram Interpretation and Modeling, Mathematical Geology, Vol. 33, No. 4, 2001

Gunter, G. W., Finnerman, J. M., Hartmann, D. J., Miller, J. D., 1997, Early determination of reservoir flow units using an integrated petrophysical method, SPE 38679 in Annual Technical Conference and Exhibition Proceedings: Society of Petroleum Engineers, p. 373-380

Hosseini, S., Zahid, K., Solano, S., Nuñez-Lopez, V., Hovorka, S., Gulf Coast Carbon Center Interim report: Monitoring Verification and Accounting Subcontracted Work for the "Lake Charles CCS Project", August 2011

Howard, R. A. Information Value Theory, IEEE Transactions on System Science and Cybernetics, August 1996, Vol. 2, Issue 1, p. 22-26

Howard, R. A., Decision Analysis Manuscript (in progress), June 2005

Howard, R. A., Matheson J. E., September 2005. Influence Diagrams. Decision Analysis, Vol. 2, No. 3, pp. 127-143

Humphreys M., Shrivastava, P., Choosing an exploration drillhole spacing: A case study in an iron mine, E.Y. Baafi and N.A. Schofield editors, Geostatistics Wollongong 1996, Volume 2, 780-791

Intergovernmental Panel on Climate Change (IPCC), Carbon Dioxide Capture and Storage, 2005

International Energy Agency, Energy Technologies Perspectives, 2010

Isaaks, E. H., Srivastava, R.M., An Introduction to Applied Geostatistics. Oxford University Press, 1989

Juanes R., MacMinn C. W., Szulczewski M. L., 2010, The Footprint of the CO2 plume during Carbon Dioxide Storage in Saline Aquifers: Storage Efficiency for Capillary Trapping at the Basin Scale. Transport Porous Media (2010) 82:19-30

Keating G. N., Middleton R. S., Stauffer P. H., Viswanathan H. S., Letellier B.C., Pasqualini D., Pawar R.J., Wolfsberg A. V., 2011, Mesoscalse Carbon Sequestration Site Screening and CCS infrastructure Analysis. Environmental Science Technology, 2011 34, 215-222

Kravchenko, A. N. Influence of Spatial Structure on Accuracy of Interpolation Methods. Soil Science Society of American Journal. 67:1564-1571 (2003)

Kumar, R., Hara, S. K. Value of Information for Appraisal of Multiple Dependent Prospects. Paper SPE 96171, October 2005, DOI: 10.2118/96171-MS

Lee, H. L., So, K. C., Tang, C. S. The Value of Information Sharing in a Two-Level Supply Chain. Management Science, Vol. 46, No. 5 (May, 2000), pp. 626-643

Mackaness W., Beard K., Visualization of Interpolation Accuracy, University of Main, NGCIA 1988

McWilliams, J. Underground Waste Management and Environmental Implications, 1972, p. 339

Milgrom P., Weber R.J. The value of information in a sealed-bid auction. Journal of Mathematical Economics. V. 10, Issue 1, June 1982, p. 105-114

Oksendal B. The Value of Information in Stochastic Control and Finance. University of Oslo and Norwegian School of Economics and Business Administration. 2005

Prague, M., Armstrong, M., Bailey, W., Couet, B., Djikpesse, H., Wikinson, D., Galli, A. Better Value of Future Information Under Uncertainty. Paper SPE 103028, September 2006, DOI: 10.2118/103028-MS

Repo, A. J. The Value of Information: Approaches in economics, Accounting and Management Science. Journal of the American Society for Information Science, 40 (2): 68-85, 1989

Ross, S., 2010, A First Course in probability, Prentice Hall, 8th ed., pp. 33-34

Salazar, J. M., Torres-Verdin, C., Sigal, R. Assessment of Permeability from Well Logs Based on Core Calibration and Simulation of Mud-Filtrate Invasion. Petrophysics, Vol. 46; No. 6; p. 434-451. December 2005

Salazar, J. M., Torres-Verdin C., Alpak, F. O., Habashy, T. M., Klein, J. D.. Estimation of Permeability from Borehole Array Induction measurements: Application of the Petrophysical Appraisal of Tight Gas Sands. Petrophysics, Vol. 47; No. 6; p. 527-544. February 2006

Saner, S., Kissami, M., Al Nufaili, S., Estimation of Permeability from Well Logs Using Resistivity and Saturation data. SPE Formation Evaluation, March 1997. SPE 26277

Sato, K. Value of information analysis for adequate monitoring of carbon dioxide storage in geological reservoirs under uncertainty. International Journal of Greenhouse Gas Control 5, 2011

Savage, L.J. 1954. The Foundations of Statistics. New York City: John Wiley & Sons

Schlumberger, 1991, Log Interpretation Charts: Schlumberger Educational Services, U.S.A.

Steagall, D. S., Gomes, J. A. T., Oliveira, R. M., Ribeiro, N. M. S. J., Queiroz, R. Q., Carvalho, M. R. J., Souza, C. Z. How to Estimate the Value of Information (VOI) of a 4D Seismic Survey in One Offshore Giant Field. Paper SPE 95876. October 2005, DOI: 10.2118/95876-MS

Stibolt, R. D., Lehman J. The Value of a Seismic Option. Paper SPE 25821, March 1993, DOI: 10.2118/25821 MS

Texas Rail Road Commission archives

Wagonner, J. R. Quantifying the Economic Impact of 4D Seismic Projects. SPE res Eval & Eng 5 (2): 111-115. SPE-77969-PA, DOI: 10.2118/77969-PA

Wills, H. A., Graves R. M. Information is Costly, but How Valuable is It? Paper SPE 90710, September 2004, DOI: 10.2118/90710-MS

Vita

Carlos Andres Puerta Ortega was born in Medellin, Colombia. He earned a Bachelor of Civil Engineering degree with honors in April 2001 from the Universidad Nacional de Colombia, Sede Medellin. He spent nine years working with Schlumberger in different locations around the world in the areas of operations, management and technical support. He enrolled as a Masters student in Energy and Earth Resources at the University of Texas at Austin in August 2010. He has worked as a Graduate Research Assistant with Dr. Susan Hovorka at the Gulf Coast Carbon Center through May 2012. After graduating Carlos will move to Mexico City to pursue a career in Oil & Gas business consulting.

Permanent e-mail address: puerta.carlos@gmail.com

This thesis was typed by Carlos Andres Puerta Ortega